THERMAL STRESS ANALYSIS FOR CIRITICAL COMPONENTS OF A SOLAR THERMO-CHEMICAL REACTOR

By

NIKHIL SEHGAL

A THESIS PRESENTED TO THE GRADUATE SCHOOL
OF THE UNIVERSITY OF FLORIDA IN PARTIAL FULFILLMENT
OF THE REQUIREMENTS FOR THE DEGREE OF
MASTER OF SCIENCE

UNIVERSITY OF FLORIDA

2013

To my parents, thank you both for supporting me in every possible way to help me achieve my goals and fulfill my dreams

ACKNOWLEDGMENTS

Firstly, I would like to thank my parents for their encouragement, blessings and never ending support which has helped me achieve one of the most cherished dreams of my life- to study in USA and participate in cutting edge research. I would like to thank Dr. James Klausner for taking me on as a master's student and giving me a chance to work on this wonderful project. I would also like to thank Dr. Renwei Mei for providing valuable guidance at all stages of this work. Very special thanks to Nick Au Yeung for being ever so patient, helpful and concerned over my progress in this project. Without his support I would not have accomplished whatever little results that I have managed to produce. Finally, thanks to all the members of the solar fuel team. I had taken guidance and advice from each one of them at some stage of this project. It has been wonderful working with everyone.

TABLE OF CONTENTS

page

LIST OF TABLES

LIST OF FIGURES

LIST OF ABBREVIATIONS

FCTSA	Fully coupled thermal stress analysis
FEA	Finite element analysis
RT	Room temperature
STCR	Solar thermo-chemical reactor
STSA	Sequentially coupled thermal stress analysis
TSA	Thermal stress analysis
ε_{ij}	Total strain in the ij direction
$\varepsilon_{ij}^{\ e}$	Strain due to mechanical forces in the ijth direction
$\varepsilon_{ij}^{\ T}$	Strain due to thermal forces in the ijth direction
G	Shear Modulus
σ_{ij}	Total stress in the ijth direction
ν	Poisson's ratio
δ_{ij}	Kronecker delta
E	Young's Modulus
τ	Temperature difference with respect to the stress free temperature
μ	Lame's Constant
λ	Lame's constant
β	Thermal coefficient
F_i	Body force in the ith direction
u_i	Displacement in the ith direction
k	Thermal conductivity
ρ	Density

c_v	Specific heat at constant volume
R	Gas constant
T_0	Initial temperature
$\bar{t}$	Normalized time
$\bar{\sigma}$	Normalized stress

Abstract of Thesis Presented to the Graduate School
of the University of Florida in Partial Fulfillment of the
Requirements for the Master of Science

THERMAL STRESS ANALYSIS FOR CRITICAL COMPONENTS OF A SOLAR THERMO-CHEMICAL REACTOR

By

Nikhil Sehgal

May 2013

Chair: James Klausner
Cochair: Renwei Mei
Major: Mechanical Engineering

Two major components, namely the absorber tube and the back plate, of a high flux solar thermo-chemical reactor (STCR) has been analyzed for thermal stresses which arise due to high amount of variation in temperature field over the component during the operation of the reactor. The commercially available finite element analysis (FEA) code ABAQUS is used for this purpose. Experiments were also conducted in the solar simulator facility at UF to test the response of the proposed design of a STCR to thermal shock.

Using a Monte-Carlo ray tracing software flux mapping for various designs of a STCR was simulated. Based on the flux maps a multi horizontal tube arrangement was chosen for analysis. Temperature distribution over the absorber tubes were obtained from a radiation-conduction heat transfer code. Using this data as the input for thermal stress analysis (TSA) simulations were run for 3 different tube diameter and two different ceramic materials. Currently, the analysis uses published standard material properties. Effects of creep, viscoelasticity and pre-existing flaws have been neglected. The simulations presented in this thesis focus on that phase of operation of the STCR

when redox reactions take place. Simulations predicted that alumina tubes of 25.4 mm diameter do not exceed critical stress values when the temperatures were cycled at a low rate. However, alumina tubes of 50.8mm and 76.2 mm diameter are predicted to exceed the critical stress values. For SiC tubes of 25.4 m and 50.8mm O.D stresses predicted were under critical stresses while the 76.2mm tube is predicted to exceed the critical stress. Finally, an alumina back plate is predicted to have large stress concentration in some areas.

When experiments were conducted at solar simulator with one alumina absorber tube of 25.4 mm O.D/19.0 mm I.D the tube did not appear to have cracked after inspection. The back plate developed several cracks. Moreover, the data for the temperature at the inside of the tubes is acquired which can be used to further refine simulation results.

CHAPTER 1
INTRODUCTION

Motivation

Today, the technology for using concentrated solar radiation to drive redox reactions for producing compounds which can either be used directly as a gaseous fuel or further converted into liquid fuel has been the subject of extensive research in the past few years. An important part of this research has been the design of high heat flux solar thermochemcial reactors (STCR). Various designs STCR have been proposed by different research groups. The designs are driven by two primary considerations: (i) favorable temperature for chemical reactions and (ii) robustness of the design against thermal shock. Since the reactors operate at temperatures as high as 1600^{o} C, failure of material due to thermal shock and thermal fatigue becomes a concern. The ability of the reactor material to withstand thermal shock also directly impacts the production of fuel since the extent to which a material is resistant to thermal shock limits the rate of cycling of temperature for the two parts of a redox reaction. Therefore, it is essential to study the response of some critical components of a STCR to thermal shock. One can explore different material of construction or different sizes of the same geometry can be tested for thermal shock resistance. Another parameter of investigation is the rate at which temperatures can be cycled over the reactor components. To study the effect of these parameters on reactor design, finite element analysis (FEA) simulations for predicting thermal stresses have been carried out for different sizes and material of some components of the reactor. It is also desired to study the effect of thermal stresses on these components by conducting experiments using a solar simulator. Having the ability to the nature of thermal stresses allows improvement in the overall design of the STCR.

Literature Review

Solar Thermal Technology

Solar thermal technology, as the name suggests, converts the energy of solar irradiation into ‘thermal’ energy. The term ‘thermal’, in this context, implies to heat stored in a medium which may further be utilized to produce electricity or supply energy to a chemical reaction or stored in a thermal storage system. Solar thermal technology is one of the most promising technologies for producing clean fuel. It has several advantages over the other conventional solar photovoltaic technology. The primary advantages ([1], [2]) over photovoltaic technology are ease of large scale setup and economics. Another major advantage over photovoltaic is the option of storing thermal energy. For instance thermal energy can be stored in molten salts which can later be used to generate steam which in turn generates electricity. The heat produced can also be directly used to drive mechanical systems like Stirling steam engines, which convert thermal energy into mechanical energy. For large scale systems solar thermal is more cost-effective [3] than PV and fossil fuels such as natural gas. Other key advantage of solar thermal technology is to store the converted thermal energy to in the form of fuels which can be used to generate energy. In this way a ‘transportation’ of energy from site to source takes place.

Solar thermochemical technology is one such method of producing ‘solar fuels’ [4]. Concentrated energy is used to drive endothermic reactions which produce compounds which can be directly used as fuels, like bio fuels, or can be used to produce intermediate products, like syngas ($CO+H_2$), which are further processed to produce fuels.

There are several technological challenges in the field of solar thermal technology that are the focus of wide spread research around the world. Capturing the maximum amount of solar energy is one such challenge. For large scale production there are essentially two ways of collecting solar radiation [5]: line focus and point focus. While line focus requires lesser efforts in terms of design and maintenance, point focus can achieve higher temperatures [6]. The line focus approach is capable of achieving about half of the maximum theoretical concentration. The losses occur because of errors in parabolic shape, thermal expansion and shifting of parts etc. On the other hand point focus can achieve at least twice the concentration as that of line focus. For solar fuel production the research is two pronged [4]. One side of the research focuses on the chemistry of the endothermic reactions and the other aspect of research is the design of the reactors in which the solar energy is concentrated to produce fuel.

Solar Thermochemical Technology

Steinfield et al [7] discuss the different applications of solar thermochemical technology. Of these, the most notable is the production of solar fuels like hydrogen. The earliest work in producing solar hydrogen was using the solar energy to split the H_2O molecule. Solar thermolysis requires temperatures of the order of 2500K and the products separation at high temperature to avoid an explosive recombination. In the process of separating these gases the operation loses a considerable amount of efficiency and working at such high temperatures induces serious material constraints. Other sources of solar hydrogen have also been explored. Noring et al [8] describe the research conducted towards production of H_2 by splitting the H_2S molecule. H_2S is a highly toxic gas which is produced as a byproduct in the process of removal of sulphur from petroleum or coal. Utilizing a toxic waste to produce fuel by using a renewable

source of energy like hydrogen is a highly lucrative option. The endothermic reaction can be carried out at 1800 K and successful separation of gases has been achieved using water cooled heat exchangers. Noring et al [8] have also explored the H_2S splitting via three different mechanisms; (i) pure solar (ii) a hybrid process of solar and natural gas and (iii) the Clauss process. The results of their study indicate that the pure solar process has the potential of lowering the disposal cost of H_2S when compared to the conventional Clauss Process. The hybrid technology can further lower the cost of production of hydrogen but at the expense of increased complexity of hybrid reactor design and production of CO_2 as a byproduct.

Popular method of hydrogen production is the use of solar energy in producing solar hydrogen from reduction of metal oxides [7]. The extraction of metals from their oxides from carbothermic and electrolytic process consumes a high amount of energy which typically comes from combustion of fossil fuels which in turn produces large amount of greenhouse emissions. Therefore using concentrated solar energy to achieve the same is an appealing option. Typically the reduction of metal oxides in the absence of any reducing agent requires very high temperatures for the thermodynamics to be feasible. Alternatively, electrical work or other forms of supplementary heat, like the waste heat from process gases, can be used along with solar heat to achieve the same results. While it is possible to achieve stagnation temperatures as high as 3500K, material restrictions and efficiency requirements suggest operating the solar thermal reactors at much lower temperatures. Thus, use of reducing agent is widespread. Coke or natural gas is a popular choice as reducing agent. Steinfield et al [9] discuss the thermodynamic feasibility of reduction of metal oxides in presence of reducing agents.

Detailed calculations performed by the authors reveal that Fe_2O_3, ZnO and MgO are the only metal oxides that will yield a significant amount of free metal below 2000K. The reduction of ZnO has been one of the more widely researched chemical reactions. The two step cycle of CeO_2 /Ce_2O_3 for water splitting has been shown to have fast kinetics in a lab scale solar reactor at 2000 C [10, 11]. Mehdizade et al. [12] have conducted research on the chemical kinetics of the reduction of ferrous oxides.

Serpone et al [13] discuss the advantages of this process in that H_2 and O_2 are produced in two different steps and thus the issue of separation of gases at high temperature does not arise. In the first step the metal oxide is thermally dissociated into corresponding metal and oxygen. In the subsequent step the hydrolysis of metal produces metal oxide and hydrogen. Although this process requires high temperature, but, with the use of heat recuperation systems and highly concentrated solar heat efficiency of upto 30% can be achieved.

Since syngas is one of the chief components of synthetic fuels, including Fischer-Tropsch chemicals, ammonia etc, a lot of importance has been given to production of syngas through this technology. Biomass can be converted into biofuels or syngas using different solar thermochemical approaches [14]. Experiments show that nearly all carbon in biomass can be converted into syngas which drastically improves the ability of biomass to produce clean energy economically. Perkins et al [15] have tested the gasification of corn stover, a common agricultural by product, for production of syngas. Although they did not use a solar furnace to test the samples, an electric furnace in a controlled environment was used. The effects of water concentration, temperature, particle size were explored. Their ongoing work involves the verification of the results of

this experiment with experiments conducted in an actual solar furnace. Lichty [16] et al. have tested the gasification of biomass in a reflective cavity multitude prototype reactor. They achieved biomass conversion as high as 68%. Stamatiou et al [17] have conducted experiment on the solar production of syngas from H_2O and CO_2 via two-step thermochemical cycles based on Zn/ZnO and FeO/Fe_3O_4 redox reactions. The first, endothermic step is the thermal dissociation of the metal oxide using concentrated solar radiation as the energy source of high temperature process heat. The second, nonsolar, exothermic step is the reaction of the metal or reduced metal oxide with a mixture of H_2O andCO_2 yielding syngas (H_2 and CO), together with the initial form of the metal oxide that is recycled to the first step.

While production of solar fuels is one of the more popular applications in solar thermochemical field it is not the only one. Steinberg [18] describes the use of concentrated solar energy for upgrading the fossil fuels. Since the research in the area of producing solar fuels economically still requires considerable efforts researchers have started focusing on the interim solution. Concentrated solar energy can be used to upgrade the quality/calorific value of the fossil fuels by providing energy equal to the enthalpy of the reaction. This results in longer fuel life and hence the upgraded fossil fuels can be considered as “cleaner”. Yet another important category for solar thermochemical process is the decarbonization of fossil fuels. The underlying idea is to remove carbon from fossil fuels so that no CO_2 is released. Two methods have been proposed [17]; (i) Solar thermal decomposition of fossil fuels and (ii) gasification of fossil fuels. The thermal decomposition results in products which are easily phase separated. There is a carbon rich condensed phase and a hydrogen rich gaseous phase. The

hydrogen in the gaseous phase may be further processed to yield high purity hydrogen or high quality syngas. Since methane has the highest H-C ratio, it is a widely studied compound for thermal decomposition using solar energy. Maag et al. [19] present results of decomposing methane a solar thermal reactor. They are able to achieve 99% of methane conversion and 98% of hydrogen yield. The solar to chemical efficiency of their reactor is reported to be an average of 9.1 % with peak efficiency reaching the values of 16%. These values can be considered as highly promising since the typical design efficiency target for solar thermal reactors is 20%. Further studies by Mier et al.[20] have explored the nano structure of the carbon produced when different catalysts are used in thermal decomposition of methane. Both of the methods have their advantages [17]. The biggest advantage of thermal decomposition is that it is able to achieve a complete separation of carbon from gaseous product in a single step whereas gasification requires additional step of converting CO into CO_2 and subsequent removal of CO_2. On the other hand thermal decomposition has a large energy penalty associated with carbon sequestration. This in turn is primarily dependent on the type of feedstock used. For solid carbonaceous materials like coal the residual energy after decarbonization may not be sufficient for an industrial application. But with hydrocarbons with high H_2/C ratio this method may be preferred. Additionally, gasification of solid fuels like coal into liquid fuels can improve the efficiency (of generating electricity in steam turbine) by 20%. Synthesis of chemical commodities by using solar energy in endothermic reactions has also been explored.

At the heart of a solar thermochemical process is a solar thermal reactor- the furnace where chemical reactions take place. Much research has gone into the design and development of different types of solar thermal reactors.

Solar Thermochemical Reactors

Solar thermochemical reactor can be thought of as a device in which the solar energy is concentrated and retained for long enough time to produce the desired energy conversion. The type and characteristics of a reactor depends upon various factors such as, the material of construction chosen, the size and type, the kinetics of the chemical reaction to be performed and other such important parameters. Steinfield et al[2] have classified the reactors into two broad categories, namely, (i) Indirectly-Irradiated reactor (IRR) and (ii) Directly-irradiated reactor (DIR). The chief difference, as the name suggests, is the way the solar irradiation is directed towards the reactants. In the Indirectly- Irradiated reactor the reactants are in a tube or other similar cavity and the irradiation hits the opaque walls of the reactor tubes. Heat is transferred through conduction into the opaque wall to the reactants. The Directly-Irradiated (DIR) reactor in contrast allows the solar irradiation to fall directly on the reactants. The biggest disadvantage of this type of arrangement is the presence of a transparent window which imposes serious design constraints. A few prototypes have been developed around the world. A description of a select few is as follows:

Palumbo et al [21] discuss one type of DIR called ROCA (short for Reactor Closed to Air). The reactor kinetics involves the thermal dissociation of the ZnO(s) into Zn(g) and O_2 at temperatures above 2000K. It consists of a conical rotating vortex cavity and a transparent window which allows the irradiation to hit the reactants directly. The reactor aims at concentrating enough solar irradiation to achieve a temperature of

2000K and higher. Hirsch et al [22] report a decomposition of methane in the same vortex reactor while reaching a nominal temperature of 1600K. The Sandia National Laboratory [23] has developed another type of DIR called the CR-5 (Counter Rotating Ring Receiver Recuperator Reactor). The reactor consists of counter rotating rings with the reactive metal oxide filled between them. One side of the reactor is undergoing reduction and is exposed to the concentrated radiation and has significantly higher temperature. The material in the other set of rings is turned away from the solar radiation and is at a lower temperature for undergoing oxidation. Although this type of reactor achieves high temperature, it does require a separate cooling mechanism to cool the reactor area around the window. Additionally, the authors report that frequent cleaning of the window was required.

Another attractive design for the reactor is that of a cavity type reactor. This type of design aims at capturing a solar irradiation, coming through a small aperture, in the cavity. The idea is to simulate a black body type geometrical arrangement in which a high percentage of solar radiation are reflected within the cavity and result in raising the temperature of the absorber tubes. There have been a few designs proposed for the Indirectly-Irradiated reactors. One type of indirectly irradiated 10kW solar reactor for thermal decomposition of methane has been proposed at CNRS France [24]. It is a double cavity reactor with the inner cavity completely covered with insulation. Within the inner cavity there are graphite tubes in which process gases enter and the reaction takes place. However, the reactor still consists of a window to capture radiation. This window and the associated cooling mechanism can perhaps be avoided by choosing the appropriate cavity to aperture ratio. The appropriate ratio will bring the whole system

closer to approximating a perfect black body. This ratio is discussed by Piatowski et al [25] for a single cavity type reactor. They concluded that a value of 0.6 for the ratio resulted in least amount of re-radiation losses through the aperture. Melchoir et al [26] discuss the design and of one such reactor. The reactor consists of a tubular cavity with an aperture to capture the solar irradiation as well as a compound parabolic concentrator placed at the aperture to help further concentrate the solar irradiation. Once again, the thermal decomposition of ZnO is chosen as the chemical reaction of interest. The reactants are placed inside smaller cylindrical tubes placed inside the cavity. Using Monte Carlo ray tracing methods the authors experimented with the number of reactor tubes, the ratio of cavity size to aperture size, the distance of the reactor tubes from cavity. It was found that there is an optimum ratio of the aperture size to that of the cavity. While increasing cavity size increases loses via conduction/convection, decreasing the aperture size relative to the cavity size tends to make the cavity more like a 'perfect black body'. Similarly, the authors found that there is an optimum distance from the aperture where the reactor tubes should be placed so as to have maximum temperature on the surface of the absorber tubes. Thus, for a design of a small scale prototype reactor a windowless approach may be considered as advantageous form the point of view of minimalistic design considerations and ease of maintenance. In fact, these issues may be compounded in a larger size reactor and may offset the energy efficiency benefits of directly irradiated reaction. Yet another type of small windowless reactor design is discussed by Meier et al [26a] for the endothermic calcinations at above 1300 K. The cavity is placed horizontally and the absorber tubes are laid along the periphery of the cavity wall. With the simplified design for a prototype

the authors foresee no major technical difficulties in scaling up the reactor to power levels of 0.5-1 MW.

Literature on the detailed design procedure for respective reactors is largely missing. Most literature focuses on the performance of different designs. Palumbo et al [21] discuss the general methodology for designing a solar thermal reactor. They lay out a three step approach to optimize the design of the reactor. These are, (i) establishing the kinetics of the chemical reaction; (ii) develop a reactor concept that meets the mechanical boundary condition of being scalable. That is the reactor must have a minimal start up time when the sun is available and secondly, owing to the transitory nature of the solar energy, it must withstand thermal shock. Finally, (iii) model the reactor concept in order to evaluate the potential performance of the scaled up project. The output from this step is temperature and gas production rate, preferably as a function of solar energy input. If these results are unacceptable one returns back to step (ii). Otherwise a test reactor model is built ad experiments are conducted. In the discussion of a cavity type reactor Melchoir et al [27] discuss about the effects basic parameters like cavity diameter, tube diameter and tube arrangement have on the radiative flux distribution and temperature distribution on the tubes.

Monte Carlo Ray Tracing Method and the Vegas Code

Monte Carlo Ray Tracing Method [28] is widely used to predict the radiative transfer for complex geometries. In this method large numbers of ray energy packages are used to approximate the radiative transfer. Each package carries the same amount of energy. These rays are emitted from the source in a direction as defined in the input file. The rays are traced to the nearest surface and on the surface it may be absorbed,

transmitted or reflected. If absorbed, it adds to the total flux on the surface otherwise it is traced again to the nearest surface.

Vegas Code developed by Jorg Petrasch [29] is a software tool which utilizes the Monte Carlo ray tracing code to model concentrating optical devices. It has been extensively used in this project to optimize the preliminary design of the solar thermal reactor based on the power incident on the reactor tubes. More precisely, in the words of the author, “Vegas is currently a simulation of radiative transfer between general geometry black and grey surfaces in participating media”. It does not include conduction and convection heat transfer effects but the results can predict radiative flux distribution. Most importantly it does not include re-radiation from a target on account of high temperatures of the target geometries. The sources and the targets are defined in an input file. The various pre-defined geometry targets can be used in different combinations to create a complex geometry. Other parameters that are required by the Vegas Code is the target position, surface reflection type and emissivity. The output is the total flux distribution on the target geometries and a visual representation of the same.

Thermal Shock in Solar Thermochemical Reactors

One of the primary concerns in design of a solar thermochemical reactor is its ability to withstand thermal shock. Since a solar thermochemical reactor undergoes drastic temperature changes, thermal shock can be a severe deterrent in the selection of material for the reactor components. This in turn can affect the whole dynamics of the heat transfer exchange in the reactor. Ceramics materials which are best suited for high temperature applications are brittle in nature and can crack easily under large thermal fluctuation. Not much literature is available on the study of the nature of thermal shock

in basic components of a solar thermochemical reactor. The data available mostly concerns the thermal shock in test specimen of different materials and the application of finite element methods to numerically estimate thermal stresses in simple geometries like a cylinder.

Analysis for estimation of thermal stress can have two approaches [30]. First is the sequential thermal stress analysis where temperature and stresses are calculated independently. The temperature field is calculated first as a function of time and position. Next, the stresses are calculated because of this temporal and spatial variation of the temperature field. The second approach involves solving the fully coupled thermoelastic equation. In this type of analysis stresses and temperature both are simultaneously solved. The FEA software ABAQUS used in this project for estimating the thermal stresses in absorber tubes, for a given the temperature distribution, is capable of performing both the analysis. Carter et al [31] compares the two approaches for estimating thermal stresses in a given system and establish a set of parameters whose values can help a designer to decide as to which approach is best suited for the given application. These parameters are solely dependent on the material properties. However for high temperature applications such as the solar thermochemical reactor the material properties itself are dependent on the temperature. Numerous data have been published [31a] to estimate the changes in properties (thermal conductivity, Young's modulus etc.) as a function of temperature.

Kandil et al [32] used FEM to simulate a sequential thermal stress problem in thick cylinders. The method solved for radial heat transfer in a cylinder when the inner wall of the cylinder was subjected to different type of temperature boundary conditions.

Once the temperature profile throughout the cylinder was calculated, based on the boundary condition, the thermal stress values were estimated. The results of this paper were used to calibrate the results of the thermal stress simulation obtained from the FEA software ABAQUS. Akiyama et al. [33] established a test procedure for determining thermal shock in solid cylinders using laser beams. This test assumed that the compressive hoop stress is the primary cause of fracture. Further Finite Element Method was used to develop a numerical model which closely agreed with the results of the experimentation. This methodology was later used to estimate the thermal shock strength of Al_2O_3 . Although the results of this study give an insight into the nature of thermal stresses the results cannot be considered as a reference for calibration. This is so because unlike Kandil et al the study assumes that compressive hoop stress as the only cause of fracture in the cylinder. In contrast, Kandil estimates the effective stress and all the individual components of thermal stress.

One of the most relevant study of this nature on a solar reactor type temperature distribution on specimen was carried out by Lichty et al [34] who studied the effects of high temperature induced tensile stresses in super alloys at the High Flux Solar Furnace at the National Renewable Energy Laboratory. However, the study did not include testing of ceramics which are the prime candidates for solar thermochemical reactors. The study concluded that the largest temperature does affect the ultimate strength of the material. For cylindrical shapes (unpublished results) the failure occurred primarily due to compressive hoop stress. This might seem to suggest that the results from Akiyama et al [33] accurately predict the nature of stresses in cylindrical objects but Lichty et al. did not comment about the temperature distribution on the cylindrical

specimen under stress and hence an accurate comparison cannot be made. Lichty et al also attempted to perform a life cycle fatigue analysis of the super alloy. However, the alloy being highly ductile did not yield in the HFSF and thus the study could not comment anything on the life cycle of the material.

Finally, additional considerations in the prediction of thermal stress and thermal fatigue in ceramics are discussed by Hasselman [35]. The material properties governing the thermal stresses in a ceramic are dependent on the microstructure, impurities and geometry of the specimen. Hence, it is advised to test the specimens to evaluate these properties before carrying out any suitable analysis. The paper also recommends taking into account any pre-existing flaws that might exist in the specimen. Finally, the paper recommends considering the phenomenon of creep for very high temperature (greater than 1200°C) applications. However, once again the author cautions against using handbook data or empirical relationship for creep data since the creep properties are highly dependent on the material's microstructure and the temperature loading of the specimen.

Outline

This thesis will present the result of simulations for thermal stresses on reactor components. The preliminary design consideration of flux distribution using Vegas Code is presented. The constitutive equations for thermal stresses are discussed. Further, the two theories of TSA are discussed and analysis is provided to choose one over the other. Results of FEA simulations using ABAQUS are presented and compared for different material and tube sizes. Finally, the thermal tests conducted at the UF solar simulator facility are detailed.

CHAPTER 2
MONTE CARLO SIMULATIONS

The Vegas Code

Solar simulator at University of Florida is a research facility used to create controllable experiments which mimic the actual operation of a STCR in a solar thermal plant. The use of a statistical Monte –Carlo ray tracing method to predict the behavior of such reactors or receivers is common. In such a method, every variable included in the simulation is defined by an individual probability distribution function (PDF). Using the PDF, a cumulative distribution function is created and then inverted. Generating a random number to be substituted into the inverted cumulative distribution function produces a value for the desired variable [36]. For instance, consider the application to STCR. A ray from a parabolic surface is traced to target geometry. Based on the known properties of the target geometry it is decided whether the ray is reflected, absorbed or transmitted. More details of this method can be found in book by Modest [28].

The Vegas code is an in-house Monte Carlo ray tracing program that is used to predict the flux distribution on target geometries in solar simulator. The Vegas Code has a complete model of the solar simulator facility at UF. It can model the seven ellipsoidal mirrors at the facility and is capable of ray tracing from these lamps. The Vegas code has an extensive library of different geometries. Complex geometries can be created by combination of these predefined geometries in the library. Figure 2-1 shows sample diagrams for ellipsoidal mirror modeling and sample geometry of a disc.

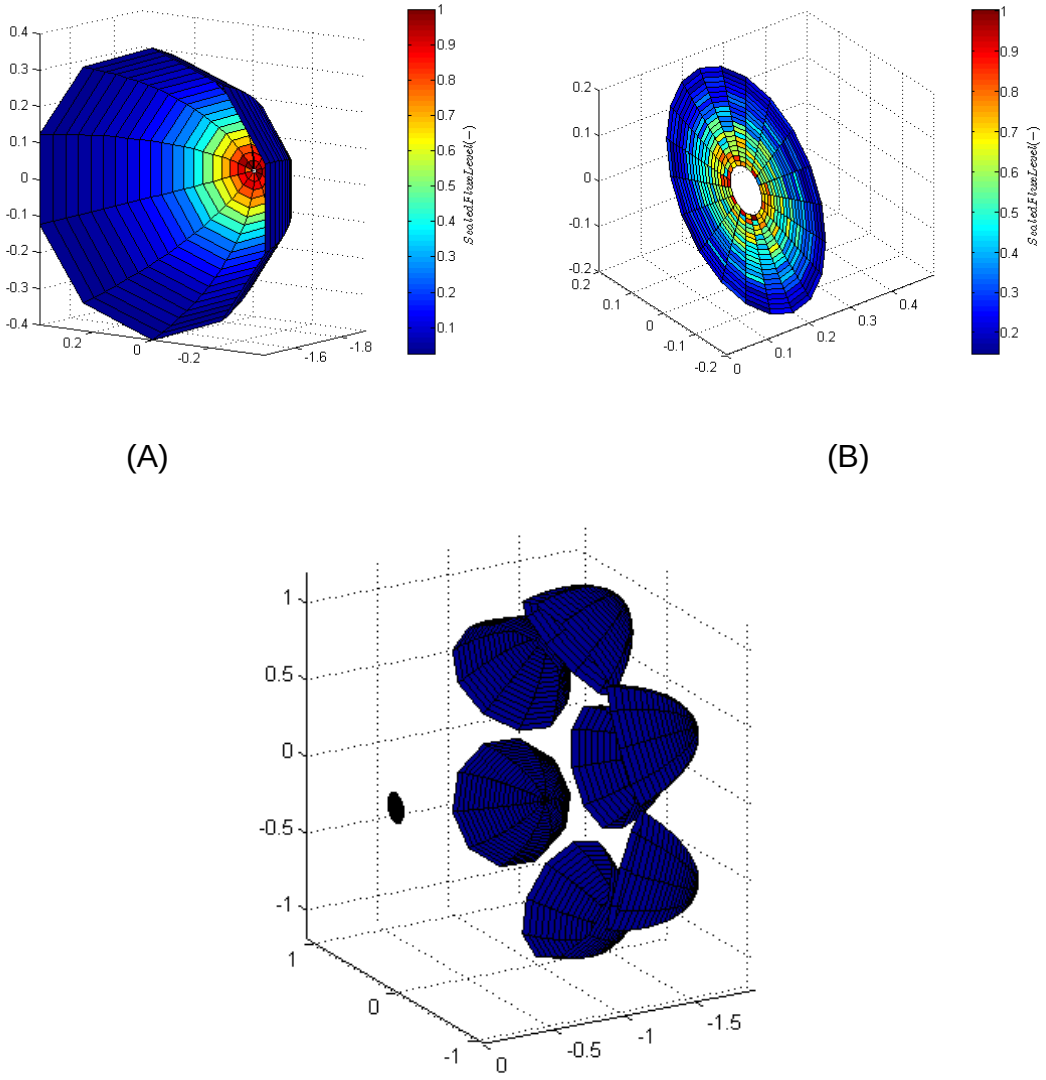

Figure 2-1. Vegas Code sample contour plots. A) 3D plots of ellipsoidal mirror. B) Simple disk geometry. C) All seven mirrors with the disc geometry.

Capabilities of Vegas Code: The Vegas Code is capable of predicting the incident flux distribution on target geometry. The primary purpose of Vegas Code is to track the path of the rays as it hits the target geometry. The resulting plots can help the user predict the spots where the maximum flux intensity lies. The sources and targets are defined in an input file. Target position, surface reflection type and emissivity are the

parameters that the user can define. The Vegas code does not calculate temperatures for the target geometries. It also does not take into account the conduction and convection heat transfer.

Monte-Carlo Simulations for STCR

With respect to thermal stresses it is desirable that the flux distribution on the absorber tubes be as uniform as possible. This will prevent large temperature gradient and hence significantly reduce the stresses arising due to thermal fluctuations. Since Vegas Code can give a good idea about the relative flux distribution these simulations are used as the starting point in analysis for predicting the nature of thermal stresses in reactor components. The basis of the first design of STCR is the vertical tube reactor at ETH [27]. This geometry was modeled in Vegas Code (Figure 2-2.) to study the relative flux distribution on the absorber tubes. Absorber tubes were placed 60% of the maximum distance from the aperture. Melchior et al. [27] have estimated this to be the optimal distribution for attaining maximum temperature on the tubes.

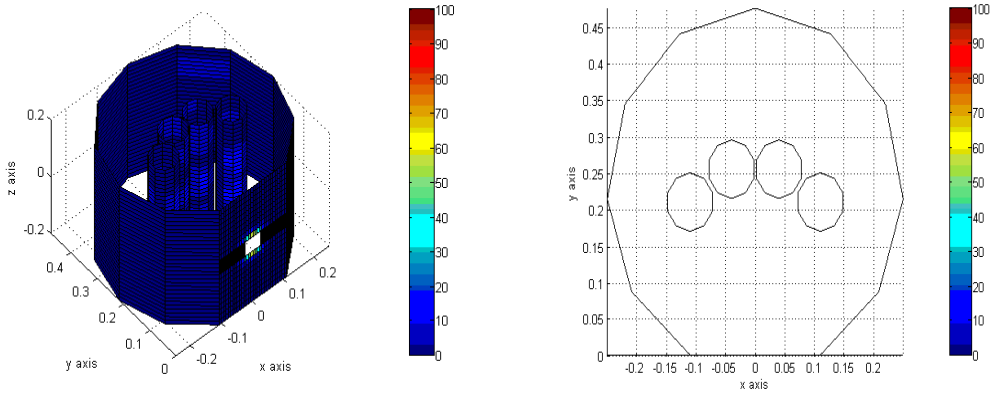

(A) (B)

Figure 2-2. A four tube vertical STCR modelled in Vegas Code. A)Isometric View. B)Top view.

Table 2-1. Input parameter for a four tube vertical STCR

Diameter of absorber tubes (m)	0.08
Diameter of cavity (m)	0.5
Diameter of aperture (m)	0.05
Material of absorber tubes	Alumina/Silica
Material of cavity	Alumina

Table 2-2. Output results for a four tube vertical STCR

Absorber Tube Material ->	Alumina	SiC
Power incident on the aperture	0.599	0.599
Power absorbed by the cavity	0.3584	0.162
Tube 1	0.061	0.105
Tube 2	0.058	0.095
Tube 3	0.058	0.095
Tube 4	0.061	0.106
Total power on the tubes	0.565	0.589

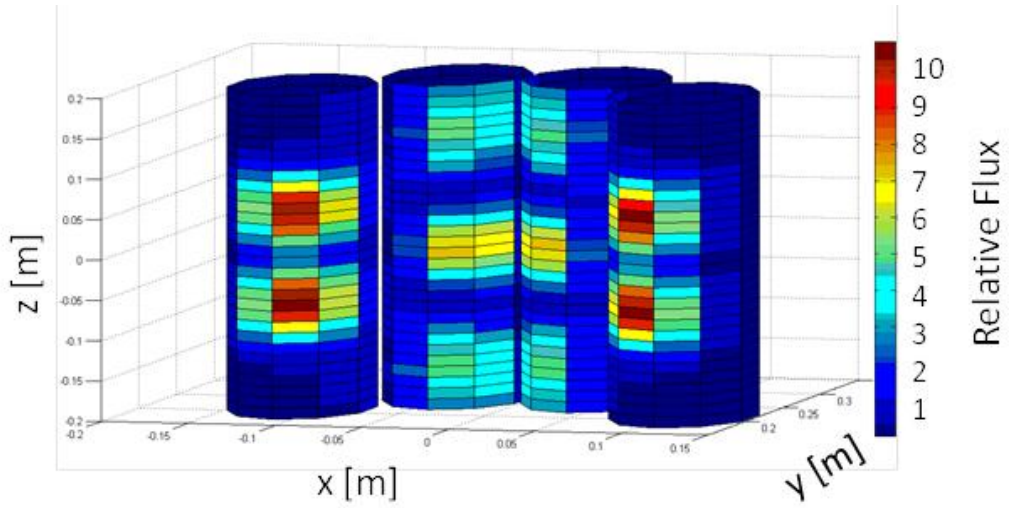

Figure 2-3. Flux distribution for a four tube vertical STCR modelled in Vegas Code

Percentage of power absorbed by individual tubes is shown in table 2-2. Also, the flux distribution on the tubes is shown in Figure 2-3. As is evident from the diagram the tubes have a poor distribution of flux with some evident hot spots.

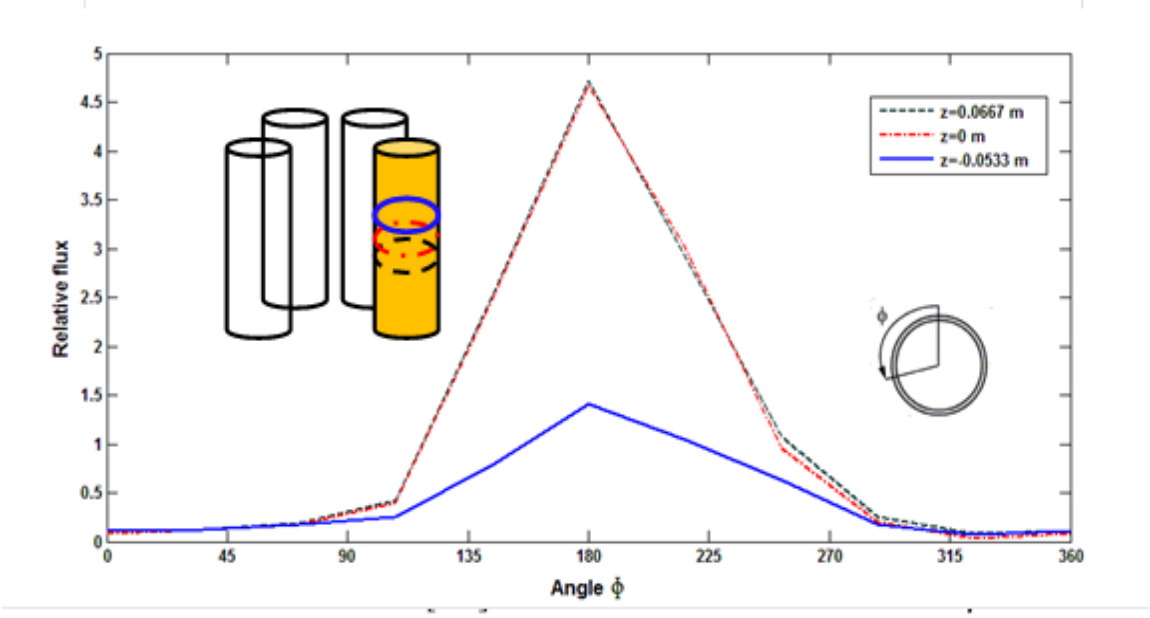

Figure 2-4. Flux distribution as a function of angle for side tube

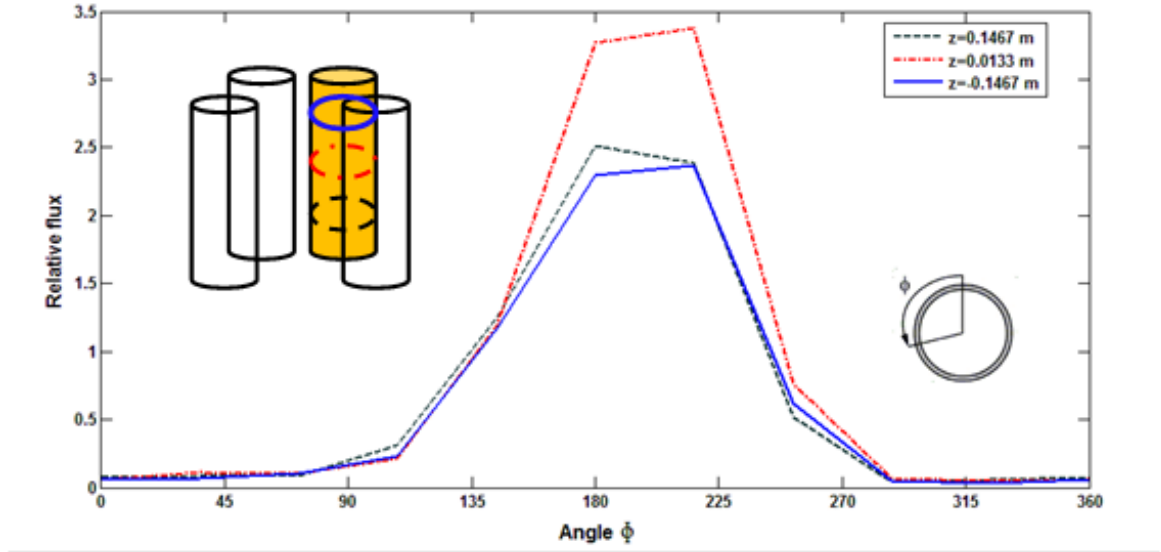

Figure 2-5. Flux distribution as a function of angle for side tube

Moreover, the cavity received a high amount of radiation which is undesirable because that heat is lost to the surrounding and reduces the efficiency of the process. Therefore, modifications in design are made with aim of improving the uniformity of flux distribution on the tubes and reducing the flux on the cavity. One way of doing that is to introduce 'deflector tubes' to scatter the incoming radiation and facilitate uniform flux. Various arrangements of deflector tubes were tried. Figure 2-6 shows the various arrangements of deflector tubes and the absorber tubes that were tried. All these trials did not produce any significant change in the flux distribution on the tubes. In fact, in some cases the power absorbed by individual tubes dropped significantly (Table 2-3).

Table 2-3. Power distribution in four tube STCR with deflector tubes

Absorber Tube Material ->	Alumina
Power incident on the aperture	0.599
Tube 1	0.032
Tube 2	0.0348
Tube 3	0.0311
Tube 4	0.0351

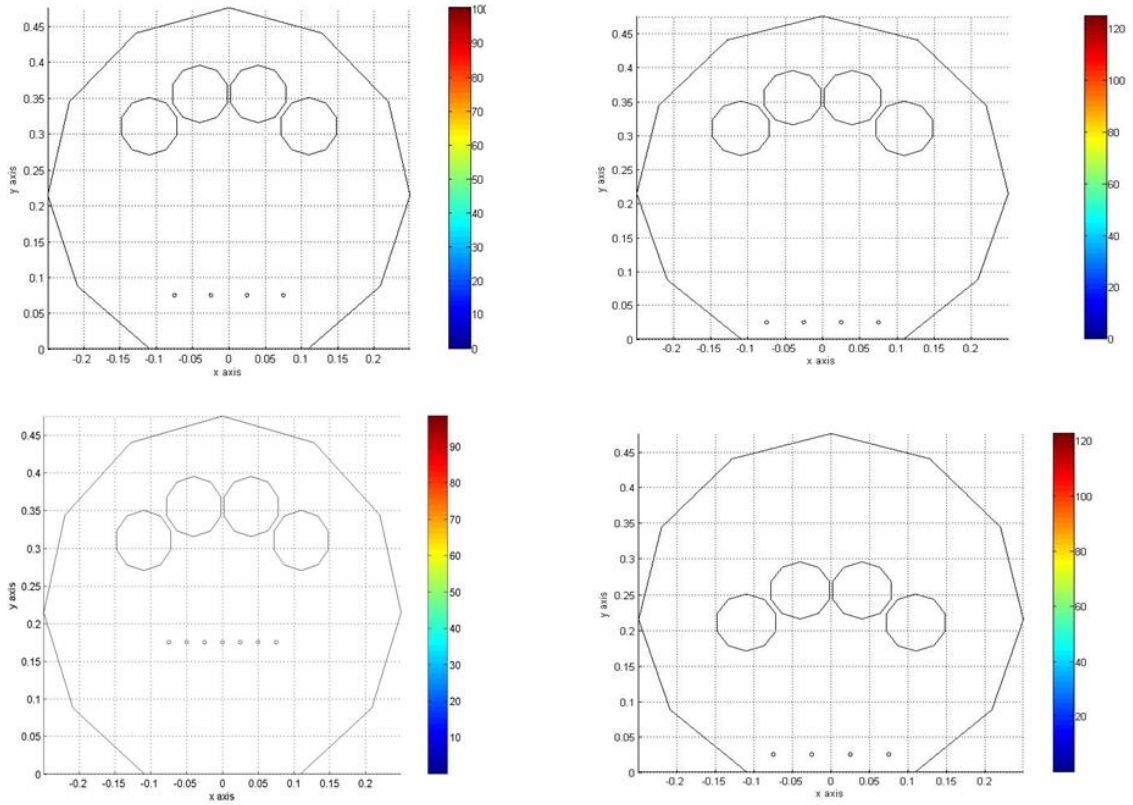

Figure 2-6. Addition of deflector tubes inside the cavity

Further trials of different tube and cavity arrangement revealed that the hot spots on the tubes cannot be eliminated completely. There are essentially seven hot spots, within any STCR design, each corresponding to one lamp in the solar simulator. However, with a horizontal type reactor, shown in Figure 2-7, the hot spot can be spread over multiple tubes. This might lead to less severe temperature gradient on the reactor tubes and thereby lead to less severe thermal shock. Another advantage of this design is that no radiation is lost to the cavity. The disadvantage of this design is that the total flux on each tube is not as high as in some of the previous cases (Table 2-3). However, experimental validation is required to check whether this arrangement can still result in favorable heat flux for chemical kinetics. Early results of the experiments in the

solar simulator (chapter 4) showed that relatively high temperature can be achieved over the surface of absorber tubes in this arrangement.

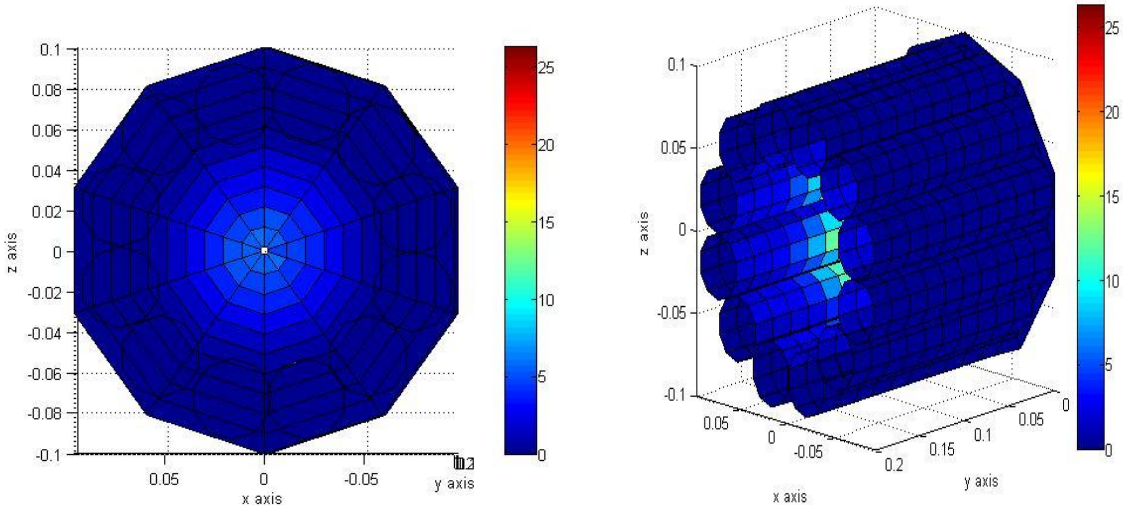

Figure 2-7. Horizontal tube arrangment for STCR. A) Back view. B) Isometric view.

As seen above there is not much of a difference in the total power absorbed by the two tube sizes. In such scenario a smaller tube size will be favorable because a smaller specimen of a given material will develop lower thermal stresses than a bigger one given that they are of the same geometric shape.

A variation of this design is the vertical arrangement of tube and cavity with deflector tubes at the back (Figure 2-8).

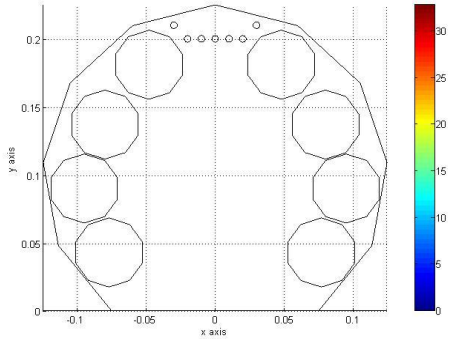

Figure 2-8. Multiple vertical tube arrangment for STCR

This design was not pursued because of predicted the tubes near the aperture of the cavity had lowest power absorption than any of the previous case (0.0269) [Figure 2-9]. Also, this design was predicted to pose greater challenges for experimental setups. Thus, a horizontal multi tube cylinder design is pursued.

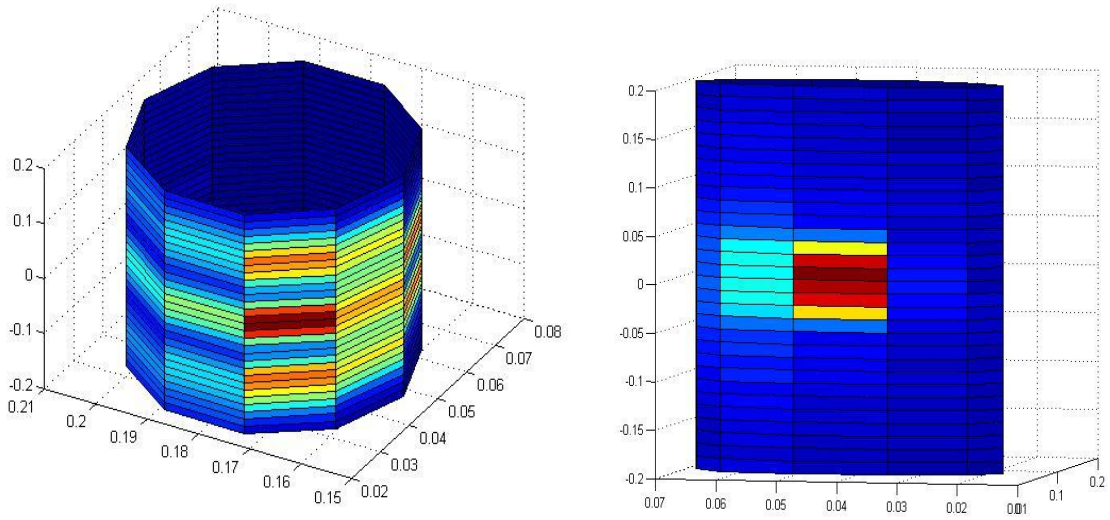

A) B)

Figure 2-9. Flux distribution on tubes for a multiple vertical tube arrangment for STCR

CHAPTER 3
THERMAL STRESSES IN REACTOR COMPONENTS

Theory of Linear Thermoelasticity

Variation of temperature field within an elastic continuum produces thermal stresses. The theory of linear thermoelasticity is based on the addition of thermal strains to mechanical strains. There is also a different class of thermoelasticity problems where the temperature and displacement appear in a coupled form in the equation. This class of problem will also be discussed. However, the main focus of this section will be the discussion of the basic theory of linear thermoelasticity.

Constitutive Laws of Linear Thermoelasticity

Classical theory of thermoelasticity states that the total strain in a component is a linear addition of strain tensor due produced by mechanical loading and that of strain tensor produced due to temperature change.

$$\varepsilon_{ij} = \varepsilon_{ij}^{\ e} + \varepsilon_{ij}^{\ T} \tag{3-1}$$

Also, by Hooke's Law for linear elasticity

$$\varepsilon_{ij} = \frac{1}{2G}(\sigma_{ij} - \frac{\nu}{1+\nu}\sigma_{kk}\delta_{ij}) \tag{3-2}$$

Therefore, we get

$$\begin{aligned}
\varepsilon_{xx} &= \frac{1}{E}[\sigma_{xx} - \nu(\sigma_{yy} + \sigma_{zz})] + \alpha\tau = \frac{1}{2G}\left(\sigma_{xx} - \frac{\nu}{1+\nu}\Theta\right) + \alpha\tau \\
\varepsilon_{yy} &= \frac{1}{E}[\sigma_{yy} - \nu(\sigma_{zz} + \sigma_{xx})] + \alpha\tau = \frac{1}{2G}\left(\sigma_{yy} - \frac{\nu}{1+\nu}\Theta\right) + \alpha\tau \\
\varepsilon_{zz} &= \frac{1}{E}[\sigma_{zz} - \nu(\sigma_{xx} + \sigma_{yy})] + \alpha\tau = \frac{1}{2G}\left(\sigma_{zz} - \frac{\nu}{1+\nu}\Theta\right) + \alpha\tau \\
\varepsilon_{xy} &= \frac{\sigma_{xy}}{2G}, \varepsilon_{yz} = \frac{\sigma_{yz}}{2G}, \varepsilon_{zx} = \frac{\sigma_{zx}}{2G}
\end{aligned} \tag{3-3}$$

Solving the system of equation for stress tensor we get

$$\begin{aligned}
\sigma_{xx} &= 2\mu\varepsilon_{xx} + \lambda e - \beta\tau \\
\sigma_{yy} &= 2\mu\varepsilon_{yy} + \lambda e - \beta\tau \\
\sigma_{zz} &= 2\mu\varepsilon_{zz} + \lambda e - \beta\tau \\
\sigma_{xy} &= 2\mu\varepsilon_{xy} \\
\sigma_{yz} &= 2\mu\varepsilon_{yz} \\
\sigma_{zx} &= 2\mu\varepsilon_{zx}
\end{aligned} \tag{3-4}$$

Here λ and μ are called the Lame elastic constant and β is the thermoelastic constant, respectively. The relationship between these constants are given as

$$\begin{aligned}
\lambda &= \frac{\nu E}{(1+\nu)(1-2\nu)} \\
\mu &= G
\end{aligned} \tag{3-5}$$

Displacement Formulation of Thermoelasticity

Displacement formulation of thermoelasticity is known as the Navier's equation of thermoelasticity. The equilibrium equations may be expressed in terms of displacement as

$$\begin{aligned}
\mu\nabla^2 u_x + (\lambda+\mu)\frac{\partial e}{\partial x} - \beta\frac{\partial \tau}{\partial x} + F_x = 0 \\
\mu\nabla^2 u_y + (\lambda+\mu)\frac{\partial e}{\partial y} - \beta\frac{\partial \tau}{\partial y} + F_y = 0 \\
\mu\nabla^2 u_z + (\lambda+\mu)\frac{\partial e}{\partial z} - \beta\frac{\partial \tau}{\partial z} + F_z = 0
\end{aligned} \tag{3-6}$$

The equations of thermoelasticity are usually solved for displacement based under the given boundary condition and the corresponding stresses and strains are then obtained from the solution of displacement at each point in the system.

Linear Thermoelasticity Reduced to Two-Dimensional

Some problems in the classical theory of elasticity may be reduced to two dimensional form for ease of solution. These solutions can be classified in two categories: plane stress or plane strain state. The following equations represent simple plane stress state

$$\begin{aligned}
&\sigma_{zz} = \sigma_{xz} = \sigma_{yz} = 0 \\
&\varepsilon_{xx} = \frac{1}{E}[\sigma_{xx} - \nu(\sigma_{yy})] + \alpha\tau \\
&\varepsilon_{yy} = \frac{1}{E}[\sigma_{yy} - \nu(\sigma_{xx})] + \alpha\tau \\
&\varepsilon_{zz} = \frac{1}{E}[-\nu(\sigma_{xx} + \sigma_{yy})] + \alpha\tau \\
&\varepsilon_{xy} = \frac{\sigma_{xy}}{2G}
\end{aligned} \tag{3-7}$$

For simple plane strain rate,

$$\begin{aligned}
&\varepsilon_{xx} = \frac{1}{E}[\sigma_{xx} - \nu(\sigma_{yy} + \sigma_{zz})] + \alpha\tau \\
&\varepsilon_{yy} = \frac{1}{E}[\sigma_{yy} - \nu(\sigma_{zz} + \sigma_{xx})] + \alpha\tau \\
&\varepsilon_{xy} = \frac{\sigma_{xy}}{2G}, \varepsilon_{yz} = 0, \varepsilon_{zx} = 0
\end{aligned} \tag{3-8}$$

Fully Coupled Thermoelastic Equations

Most problems in thermoelasticity are based on semi-coupled assumption. This means that it is assumed that the stresses developed in the component depend on the changes in the temperature field. However, the converse effect is not considered significant. That is, the temperature field in a body is independent of the changes in stress tensor. The later situation occurs when the rate of change of thermal boundary

conditions is large enough so as to cause thermal stress wave propagation. The general governing equations of coupled thermoelasticity are:

$$kT,_{ii} - \rho c\dot{T} - \alpha T_0(3\lambda + 2\mu)\dot{\varepsilon}_{ii} = -R$$
$$\mu u_{i,kk} + (\lambda + \mu)u_{k,ki} - (3\lambda + 2\mu)\alpha T_{,i} = \rho \ddot{u}_i \quad (3\text{-}9)$$

Types of Thermal Stress Analysis

Based on the two theories of thermal stresses discussed in the preceding section there are two types of thermal stress analysis that can be performed. These are: (i) Sequential Thermal Stress Analysis (STSA) and (ii) Fully coupled thermal stress analysis (FCTSA). In STSA heat transfer analysis is first carried out to calculate the temperature field in the component. In the second step the temperature field is used to estimate the residual stress values caused due to changes in the temperature field. The STSA problem only assumes a transient nature in the heat transfer part of the problem. Stresses are calculated based on the results of the transient heat transfer step. In FCTSA, temperature and displacements are calculated simultaneously based on the constitutive laws of fully coupled thermal stress analysis discussed in the preceding section.

The choice of analysis procedure is a significant one. Since in STSA the temperature and stresses are uncoupled a designer can directly use the pre calculated temperature field history to estimate the stresses in the body. This is particularly important in the case of STCR because an accurate solution of the estimation of the temperature field on the reactor tubes may not be possible using ABAQUS CAE. Therefore, choosing STSA allows the freedom to input the temperature calculated from

an external code. The ratio A/M is a deciding factor in the decision to choose either of the two methods. Here, A and M are constrained moduli corresponding to adiabatic and isothermal conditions respectively.

$$M = \frac{E(1-\nu)}{(1+\nu)(1-2\nu)} \tag{3-10}$$

and $$A = M + \frac{T_0 \alpha^2}{\rho c_v} \tag{3-11}$$

Both M and A are material properties and does not depend on the geometry of the body under consideration. It is estimated that in general that STSA is suitable for A/M< 1.5 and FCTSA otherwise. The following table shows the variation of the ratio A/M for alumina and SiC at different temperatures.

For alumina:

Table 3-1. Determination of A/M ratio for alumina

Temp	M (dimensionless)	A(dimensionless)	A/M
293	4.66E+11	4.66E+11	1
573	4.66E+11	4.66E+11	1.01
1273	4.59E+11	4.59E+11	1.01
1473	4.57E+11	4.57E+11	1.01
1673	3.50E+11	3.50E+11	1.01

For SiC

Table 3-2. Determination of A/M ratio for SiC

Temp	M(dimensionless)	A(dimensionless)	A/M
293	4.42E+11	4.42E+11	1.01
573	4.30E+11	4.31E+11	1.01
1273	4.16E+11	4.18E+11	1.01
1473	4.11E+11	4.14E+11	1.01
1673	4.06E+11	4.09E+11	1.01

The value of A/M = 1 corresponds to an uncoupled behavior. Thus from the above table it is evident for silicon carbide and alumina the thermal stresses are uncoupled in nature and hence STSA is chosen.

TSA using FEA

Most FEA formulation of thermal stress problems uses the Body Force Analogy (BFA). This method reduces the problems of thermal gradient to that of elasticity problems with body force acting on the given system. Considering the constitutive equation for a static condition in absence of mechanical body forces

$$(\lambda+\mu)e_{,i}+\mu u_{,ii}-\frac{E\alpha}{1-2\nu}T_{,i}=0 \tag{3-12}$$

$$e=\sigma_{xx}+\sigma_{yy}+\sigma_{zz} \tag{3-13}$$

Now, this problem can be considered as an isothermal problem in elasticity if the terms

$$\frac{E\alpha}{1-2\nu}\frac{\partial T}{\partial x},\frac{E\alpha}{1-2\nu}\frac{\partial T}{\partial y},\frac{E\alpha}{1-2\nu}\frac{\partial T}{\partial z} \tag{3-14}$$

are considered as equivalent components of body force and the terms

$$\frac{E\alpha(T-T_0)}{1-2\nu}n_x,\frac{E\alpha(T-T_0)}{1-2\nu}n_y,\frac{E\alpha(T-T_0)}{1-2\nu}n_z \tag{3-15}$$

are considered as equivalent components of surface traction. Therefore, one can use the commonly available FEA method to solve the thermal stress problems. A STSA in ABAQUS is solved by this methodology.

STSA in ABAQUS

ABAQUS is commercially available FEA software which has the ability to analyze thermal stress problems. It can conduct both STSA and FCTSA analysis. A STSA in ABAQUS is carried out in two steps. First a heat transfer problem is set up and nodal

temperature is calculated for the body. Next, a stress problem is set up and the time history of temperature at the node is imported from the previous analysis. Mechanical boundary conditions are applied and the problem is solved for residual stresses. It is advisable to keep the mesh (the number of elements and the nodes) unchanged for both the analyses. However, the type of elements used in the mesh must be changed. ABAQUS uses different type of elements for stress and heat transfer analysis. In the event that the number of nodes in the two analyses is unequal ABAQUS interpolates the results for the missing nodes.

Validation of results of ABAQUS STSA: To verify the results of STSA method in ABAQUS a comparison was made between the results of ABAQUS and an external FEA code for a simple plane strain problem.

- The problem consists of a 2D hollow cylindrical body where temperature boundary conditions are varied at the interior surface. The external code solves a transient heat transfer problem and calculates the resulting stress as a function of radius and time.
- The temperature of the cylinder is considered to vary only in the radial direction.
- The longitudinal strain is uniform and constant. That is this is a plane strain condition. Where $\epsilon_z=0$.
- The material properties of the cylinder material are assumed to be constant and do not vary with temperature.

For simulation in ABAQUS a quarter of the geometry was chosen since the geometry is axisymmetrical. Since the heat flow is only in the radial direction, the ends of the quarter cylinder were assumed to be insulated. The appropriate boundary condition was applied at the inner radius.

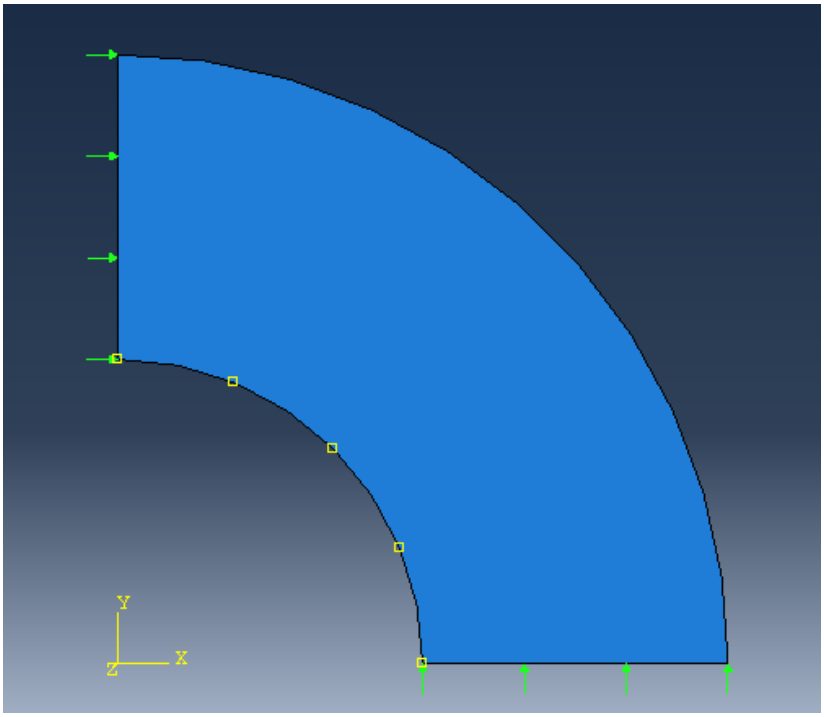

Figure 3-1. Axisymmetric cylinder with radial heat transfer model in ABAQUS

The plots for normalized temperature variation w.r.t to the normalized time for different normalized radii are shown for the external code (EC) and ABAQUS for two different types of boundary conditions. Furthermore the plots for corresponding normalized stress are shown and the results are compared for the innermost radius of the cylindrical body. In the plots shown:

Table 3-3. List of non-dimensional parameters.

normalized radius	$R = \frac{(r - r_i)}{(r_O - r_i)}$
normalized temperature	$T = \frac{(T - T_i)}{(T_W - T_O)}$
normalized time	$\bar{t} = \frac{\alpha t}{(r_O - r_i)^2}$
normalized stress	$\bar{\sigma} = \frac{\sigma(1-\nu)}{E\alpha(T_W - T_O)}$

T_0 is the reference temperature. This is the temperature from which all ΔTwill be calculated for stress analysis. In the current simulations T_0=300K.

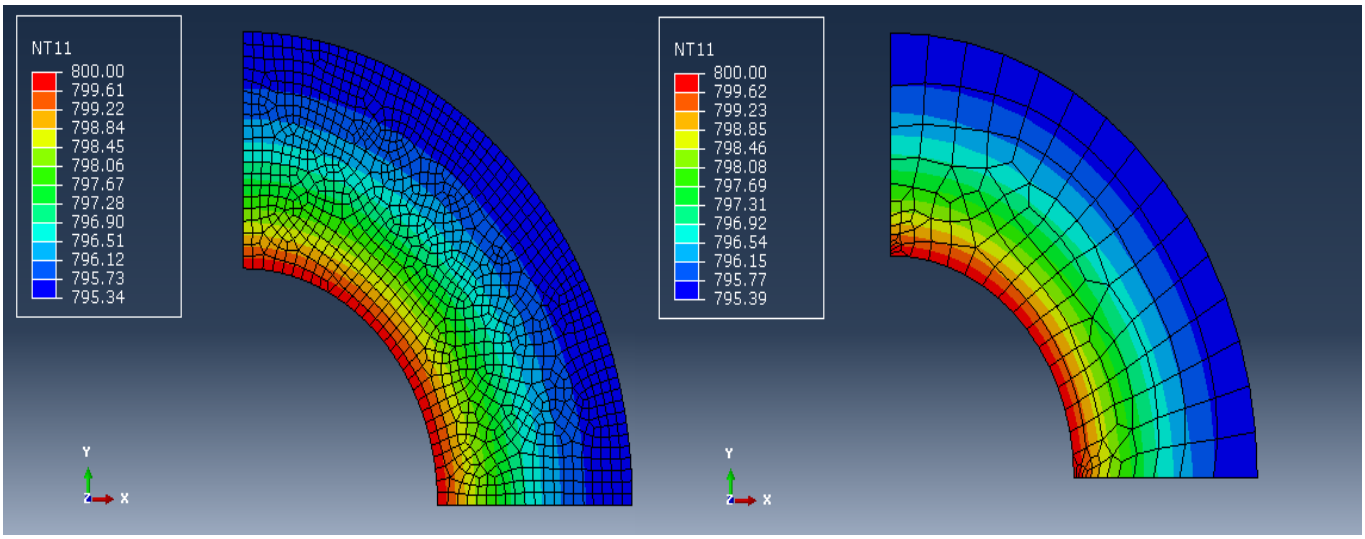

Figure 3-2. Quarter cylinder heat transfer result for two different mesh sizes

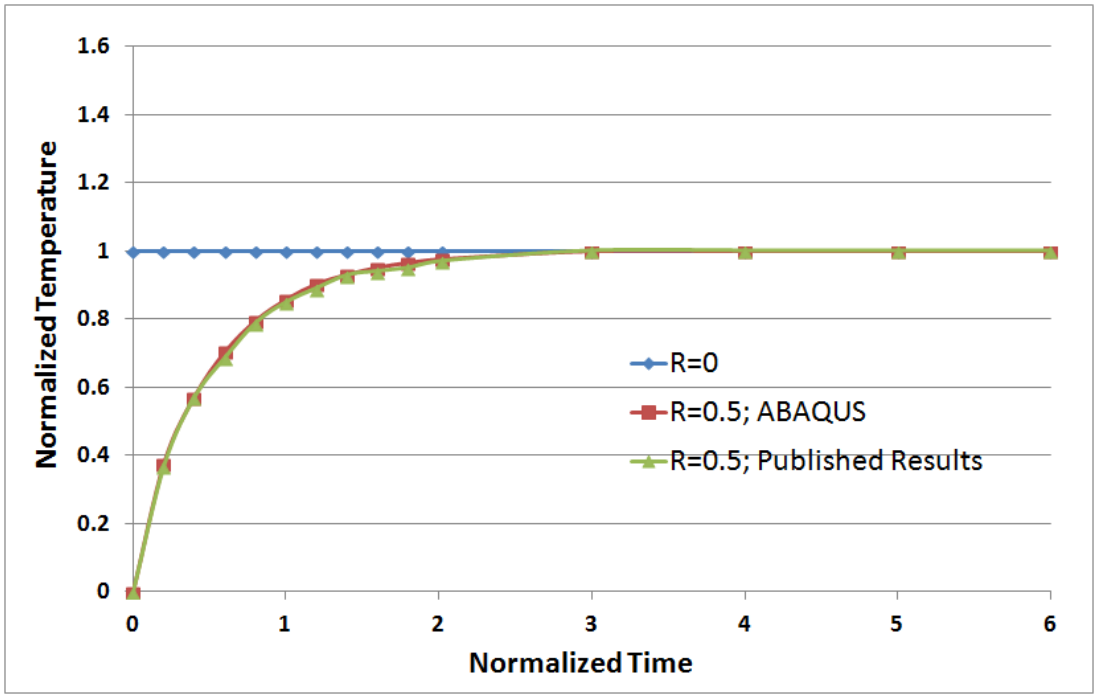

Figure 3-3. Comparison of heat transfer analysis between ABAQUS and published results for boundary condition 1

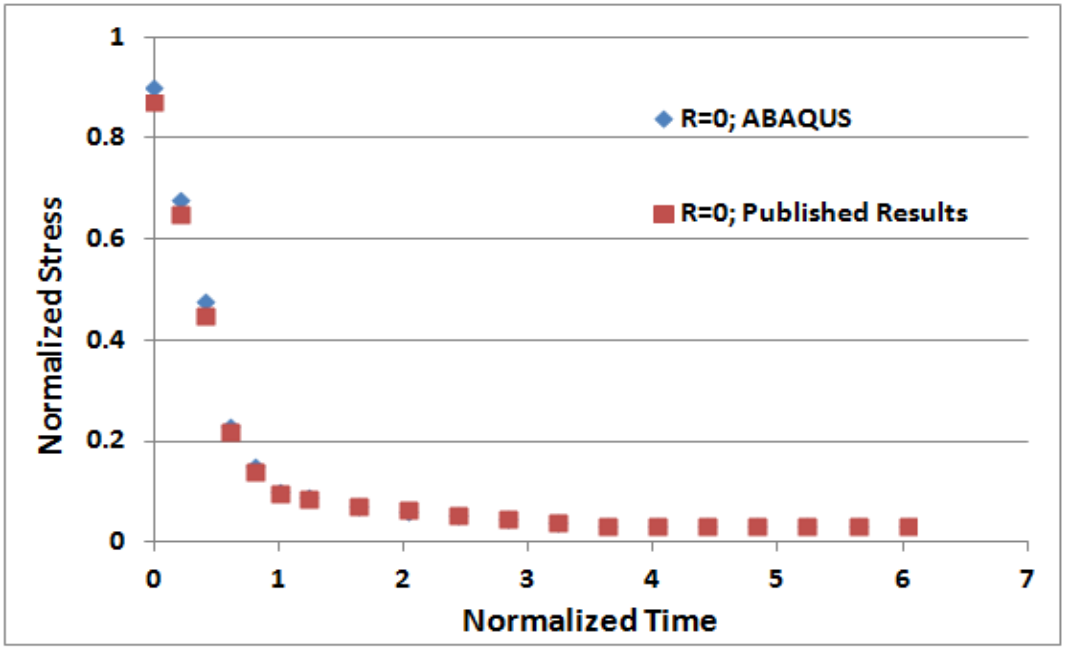

Figure 3-4. Comparison of TSA between ABAQUS and published results for boundary condition 1

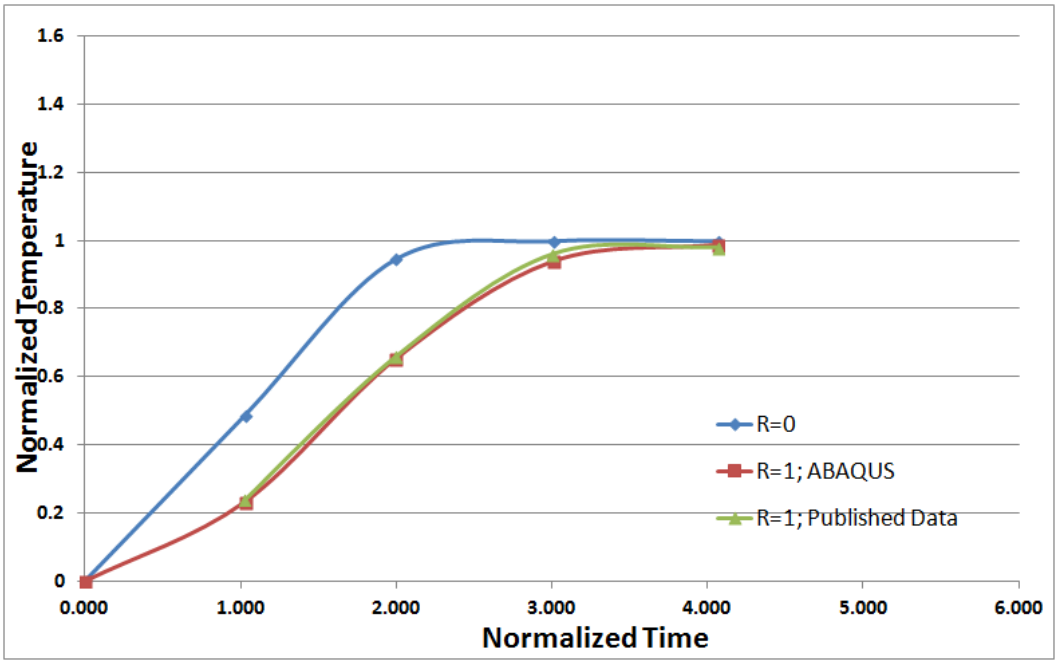

Figure 3-5. Comparison of heat transfer analysis between ABAQUS and published results for boundary condition 2

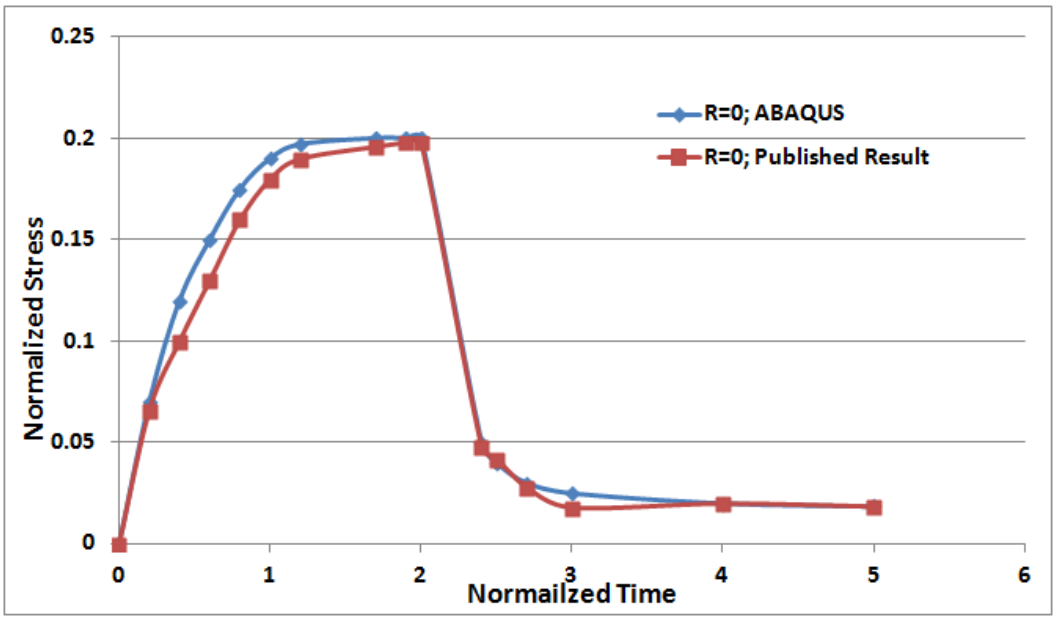

Figure 3-6. Comparison of TSA between ABAQUS and published results for boundary condition 1

There is a good degree of agreement between the two results and thus it is henceforth assumed that the STSA results from ABAQUS are accurate.

STSA in ABAQUS for Reactor Tubes

The procedure discussed above is now carried out for the reactor tubes of STCR. Currently, STSA is divided into three parts:

- Stage 1: Heating up to the cycling temperature: This stage is the rise of temperature from RT to the stress free temperatures. Stage 1 can be considered as an event which happens once every day when the STCR is started.
- Stage 2: This is the cycling process between 1200°C to 1600°C. Stage 2 is the main focus of the study since the reactor will operate on this mode for most of the time. Although the minimum and maximum stress values may not change substantially at each cycle, this stage is the most important when considering the thermal fatigue in the reactor tubes.
- Stage 3: This is the stage where the reactor tubes are cooled from 1200°C to RT.

At present, since the nature of surface temperature at the start of cycling process is known, reasonable assumptions can be made for stage 2 to carry out TSA. Thus, this study covers thermal stresses and fatigue calculated only for stage 2.

Material Properties

Two ceramics are considered –alumina and silicon carbide. The material properties used for TSA are Young's Modulus (E), Coefficient of thermal expansion (α), Poisson's Ratio (v), Density (ρ), Specific Heat (c). These properties are a function of temperature. The variation of these properties as a function of temperature is listed in the table below for sintered alumina and sintered silica carbide:

Table 3-4. Properties of alumina and SiC at different temperatures

Property [unit]	20 °C	500 °C	1000 °C	1200 °C	1400 °C	1500 °C
			Al_2O_3			
Density [g/cm3]	3.984	3.943	3.891	3.868	3.845	3.834
Elastic Modulus [GPa]	416	390	364	354	343	338
Poisson's Ratio []	0.231	0.237	0.244	0.247	0.25	0.252
Specific Heat [J/kg·K]	755	1165	1255	1285	1315	1330
Thermal Conductivity [W/m·K]	33	11.4	7.22	6.67	6.34	6.23
Thermal Expansion (m/m)	4.6	7.1	8.1	8.3	8.5	8.6
			SiC			
Density [g/cm3]	3.16	3.14	3.11	3.1	3.09	3.08
Elastic Modulus [GPa]	415	404	392	387	383	380
Poisson's Ratio []	0.16	0.159	0.157	0.157	0.156	0.156
Specific Heat [J/kg·K]	715	1086	1240	1282	1318	1336
Thermal Conductivity [W/m·K]	114	55.1	35.7	31.3	27.8	26.3
Thermal expansion (m/m)	1.1	4.4	5	5.2	5.4	5.5

Tube Dimensions

One of the significant parameter for a tube is its outer diameter. To facilitate heat transfer via conduction a thin tube is desirable. Therefore, the significant parameter under consideration in this study is the outer diameter of the tube. Three tube diameters

are considered as shown in the table below. Based on the results of Vegas Code simulation we are interested in finding out how larger diameter tubes perform with respect to thermal stresses.

Table 3-5. Different tube dimensions considered in simulations

Sr. No.	Parameter	Values
1	Thickness (mm)	6.3
2	Outer radius(mm)	25.4,50.8,76.2
3	Material of construction	Alumina, Silicon Carbide

Assumptions Made in STSA

- Through an in-house FORTRAN code simulations the temperature on the surface of the absorber tubes is known for a steady state at the end of reduction cycle. This temperature is a function the cylindrical coordinates Z and Φ. The temperature field serves as the initial starting point for stage 2. It is assumed that during stage 2 there is no further change in the spatial distribution of the temperature. It is only the magnitude of the temperature at each point that rises and falls during the cycling procedure.

  A polynomial surface is fit through the given data of temperature to obtain an order nine polynomial that is a function Z and Φ. The graph of the surface fit is shown in Figure 3-7 below. The polynomial has a 95% goodness of fit.

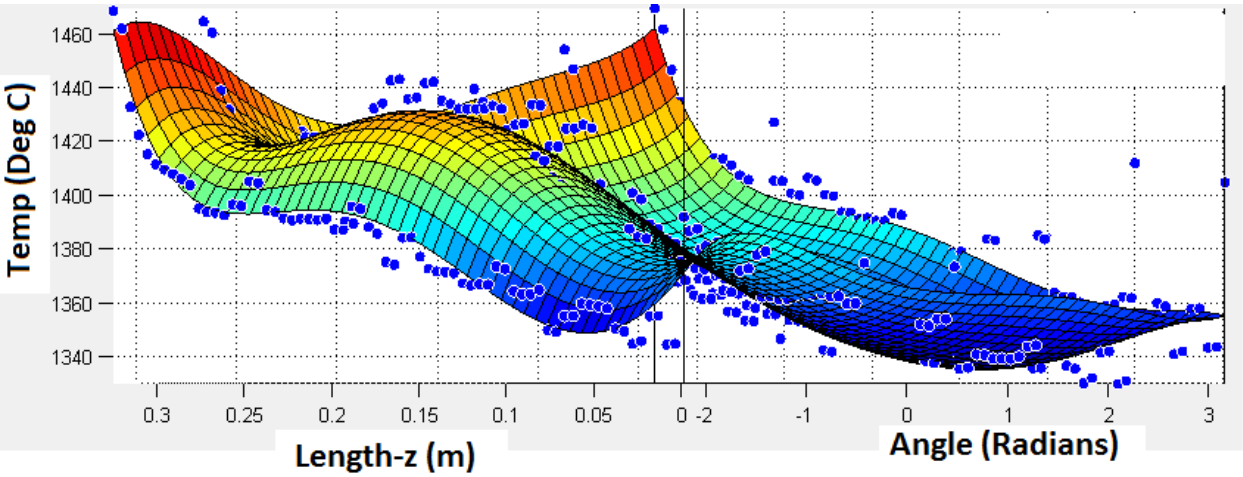

Figure 3-7. Polynomial surface fit through the data of nodal values of temperature obtained from the in-house code

The polynomial is of the form

$$f(x,y) = p_{00} + p_{10}x + p_{20}x^2 + p_{11}xy + p_{02}y^2 + p_{30}x^3 + p_{21}x^2y + p_{12}xy^2 + p_{03}y^3 + p_{40}x^4 + p_{03}y^3 + p_{40}x^4 + p_{31}x^3y + p_{22}x^2y^2 + p_{13}xy^3 + p_{04}y^4 + p_{50}x^5 + p_{41}x^4y + p_{32}x^3y^2 + p_{23}x^2y^3 + p_{14}xy^4 + p_{05}y^5 \quad (3\text{-}16)$$

where, the coefficients are

Table 3-6. Values of coefficient for the polynomial surface fit

p_{00} = 1356	p_{40} = 4.547
p_{10} = -13.84	p_{31} = -42.16
p_{01} = 159.3	p_{22} = -1448
p_{20} = 31.05	p_{13} = -1468e+004
p_{11} = -981.9	p_{04} = -3.517e+005
p_{02} = -5275	p_{50} = -0.3785
p_{30} = -18.7	p_{41} = -0.1035
p_{21} = 378.7	p_{32} =138.4
p_{12} =6077	p_{23} =846.3
p_{03} =7.591e+004	p_{14} = 1.442e+004
p_{05} = 5.319e+005	

- Temperatures are assumed to be cycled between 1200°C to 1600°C.
- It has been observed during experiments in the solar simulator that a temperature rise of 10-15°C can be achieved during the heating phase while in the cooling phase the temperature drop is faster. Hence, an average temperature change of 15°C/min and 20°C/min are considered during the heating and cooling part of the cycling stage respectively. However, it is important to note that much higher temperature changes 30 C/min -40 C/min) are desirable.
- The stress free temperature of sintered ceramics is assumed to be the average sintering temperature of that ceramic. This is because in the manufacturing of the ceramic tubes the ceramic material is sintered at high temperature. At this temperature the ceramic powder becomes viscous and by chemical processes bonds together to give a final form. Hence, at this temperature the body is free of

any thermal stresses. For alumina and silicon carbide these temperatures are assumed to be 1700°C and 2000°C respectively.

Heat Transfer Analysis

As discussed, the first step in STSA is heat transfer based on the boundary condition of assumed surface temperature. Temperature at the surface of absorber tubes are increased linearly such that the rate of rise of temperature is 15 °C/min and 20°C/min for heating and cooling part of the cycle respectively. The contour plots for three different sizes of Alumina tubes are shown below.

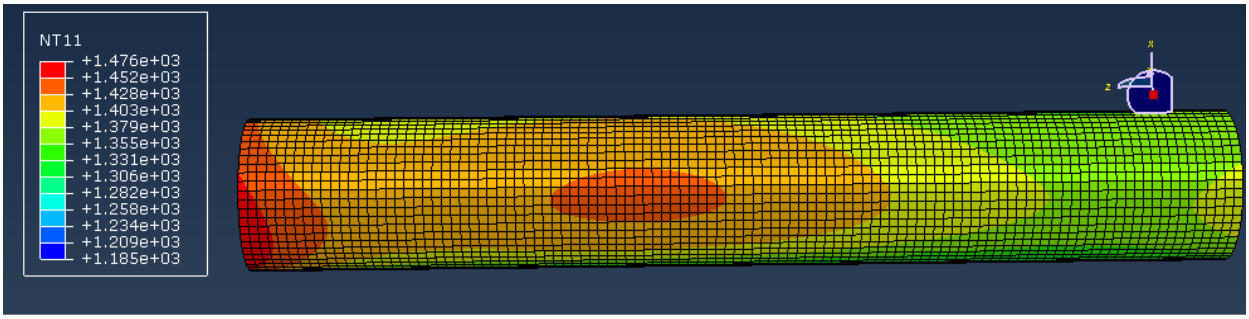

(A)

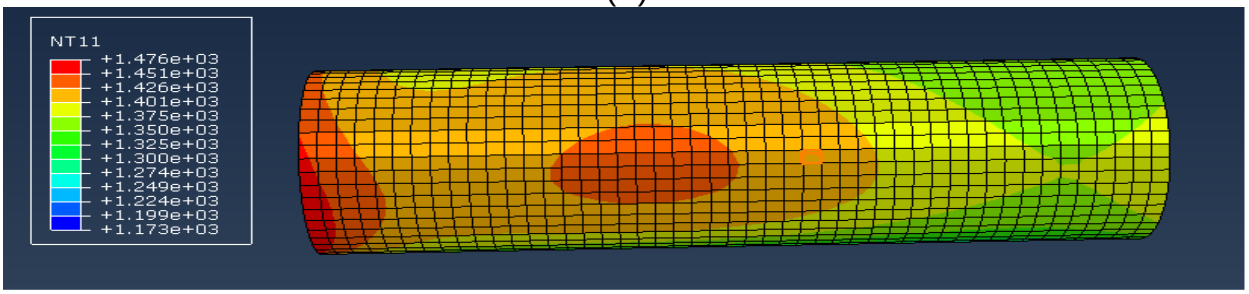

(B)

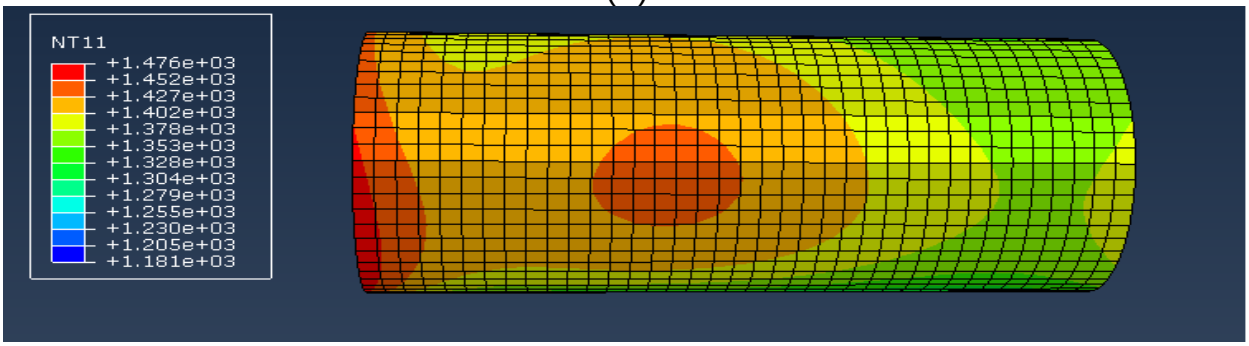

(C)

Figure 3-8. Temperature distribution on the surface of absorber tubes as calculated by the polynomial function. (A) 25.4mm (B) 50.8mm (C) 76.2mm

Transient heat transfer analysis gives the following results for the innermost radius in the tube at a given Φ and Z. The plots compare the values of temperature for alumina and silicon carbide tubes for heating and cooling phase for 25mm O.D tubes. Here, normalized temperature is the ratio of actual temperature at the node to the assumed stress free temperature of the material.

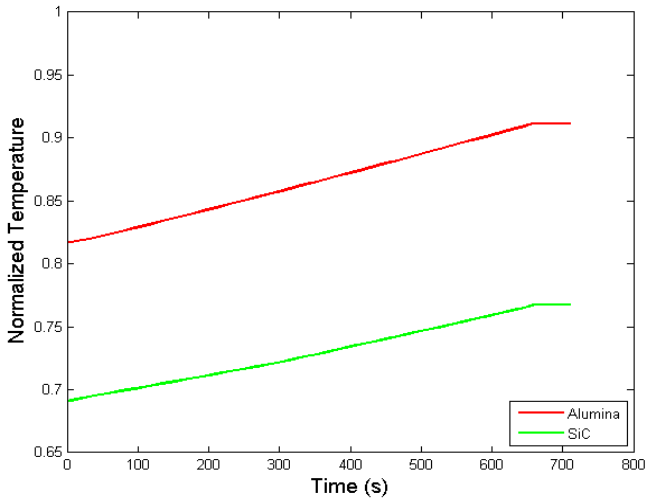

Figure 3-9. Normalized temperature for absorber tubes outer surface-Heating phase.

Similarly, the temperature profile, for the same tube, during the cooling phase is shown

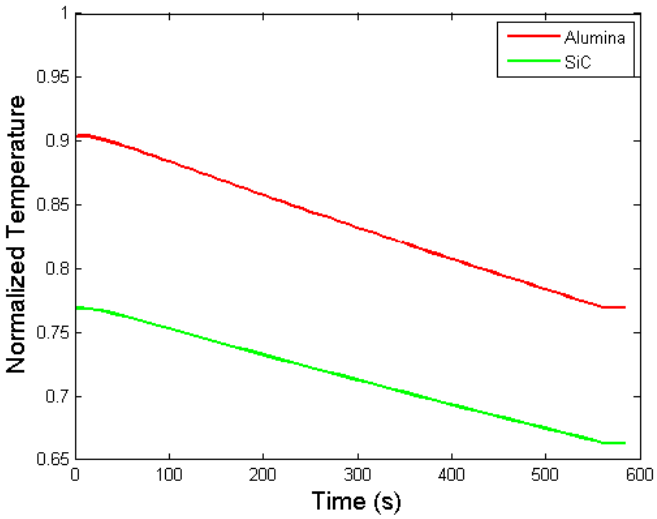

Figure 3-10. Normalized temperature for absorber tubes outer surface-Cooling phase

Stress Analysis

Based on the temperature history obtained in the heat transfer analysis the next step is to estimate the stresses in the tube. The flexural strength of alumina and silicon carbide as a function of temperature is shown in the table below. Flexural strength is the ability of material to resist deformation under an applied load. For ceramics usually the tensile strength is the low and that is considered as the safest measure of design to prevent failure. However, the advantage of using flexural strength data is that a typical flexural strength test captures different loads (compression, bending, tension and so on) acting on a test specimen at the same time. This captures the way individual component of stresses interact with each other to produce net stress on a body. A noteworthy point for SiC is that it exhibits an unusual behavior of increasing flexural strength at increasing temperatures. One reason given for this behavior is that the flexural tests are conducted in an air environment. In an air environment SiC at high temperature forms an oxide SiO_2 which in turn has the property of 'self healing of cracks'.

Table 3-7. Temperature dependence of flexural strength of alumina and SiC

Property [unit]	20 °C	500 °C	1000 °C	1200 °C	1400 °C	1500 °C
Flexural Strength [MPa]- SiC	359	359	397	437	446	446
Flexural Strength [MPa]- Al_2O_3	380	375	345	300	210	130

The normalized stresses in the three tubes for the two materials are plotted. The normalized stress is the ratio of maximum actual von misses stress at a node to that of the flexural strength of the material at that temperature. To estimate the flexural strength at different temperatures following interpolations are used for the two materials are:

For Al_2O_3

$$T = 380.5 - \frac{1.37 \times 10^5}{1 + 1.76 \times 10^5 \exp(-0.0039T)} \tag{3-17}$$

For SiC

$$T = 359 + \frac{87.6}{1 + 208600 \exp(-0.012T)} \tag{3-18}$$

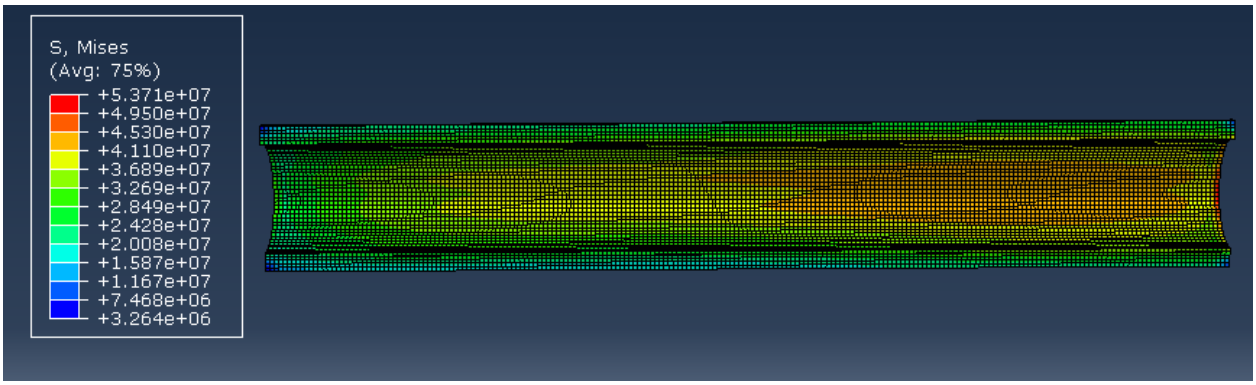

(A)

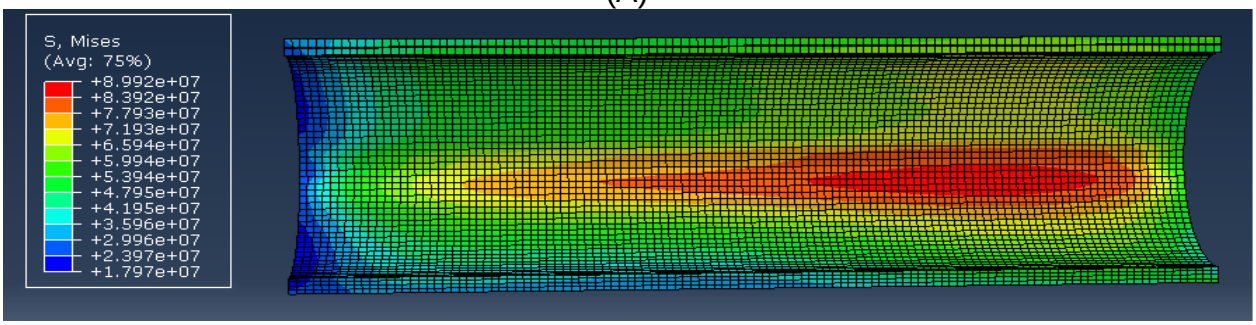

(B)

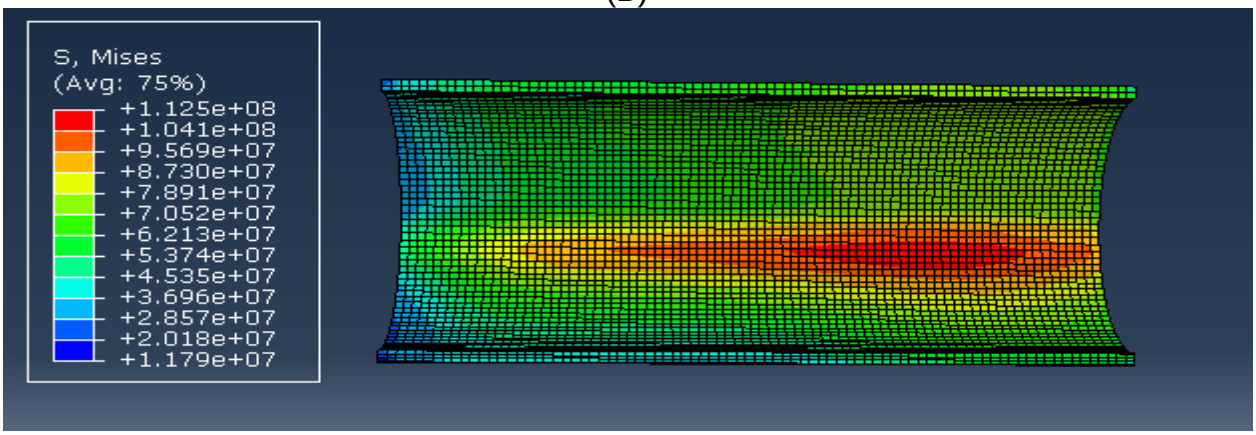

(C)

Figure 3-11. Stress distribution on the surface of alumina absorber tubes at the end of heating phase. (A) 25.4mm (B) 50.4mm (C) 76.2mm

Maximum stresses in the tubes occur at the end of the cooling period. The contours of the stress distribution, for Al_2O_3 tubes, at the end of the cooling phase are also shown. The maximum stresses occur on the inside of the tube. As expected the stresses increase with increasing size of the tube. As seen from the contour plot, for 25.4 mm alumina tubes the stresses are well below the critical stresses and hence it should be expected that the tubes do not crack during the operation. This trend was also observed during the actual experimentation at the solar simulator. Further, plots for cooling phase of SiC tubes are shown and the performances of the two materials are compared. As can be seen from the plots the stresses in SiC are well below the critical stress for all three sizes of the tubes. This suggests that bigger tubes can be used if the material of construction is SiC.

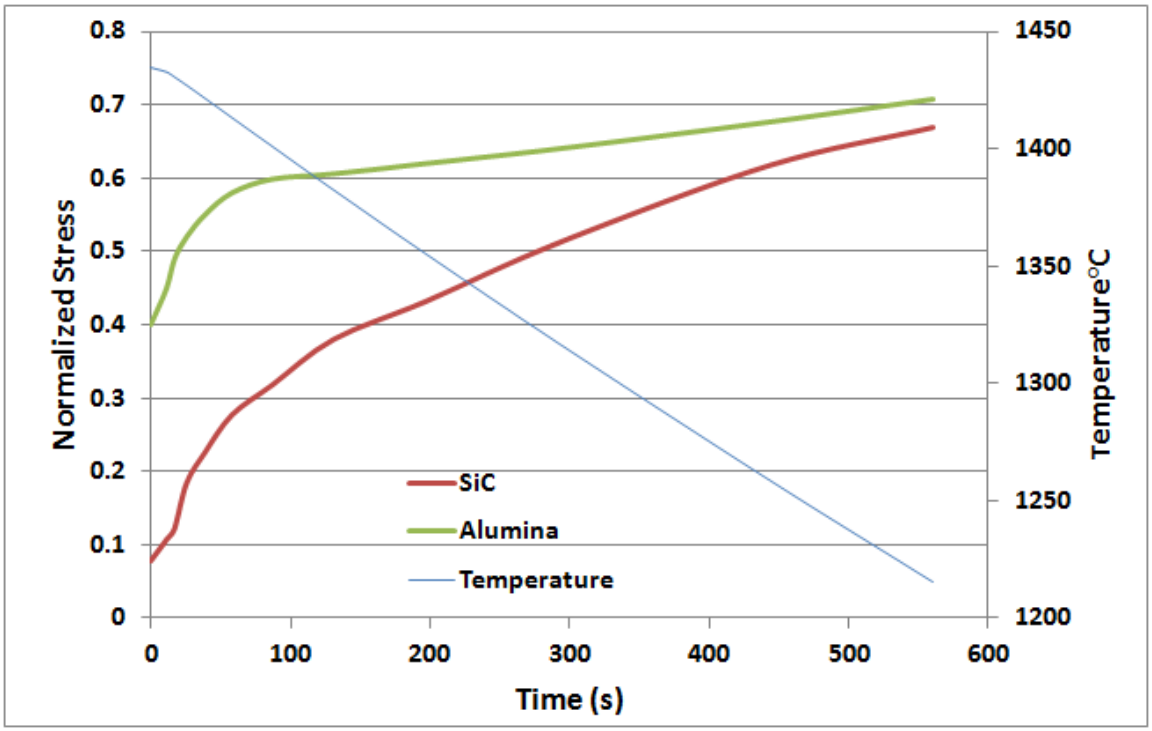

Figure 3-12. Comparison of stress developed for 25.4mm tubes –Cooling Phase

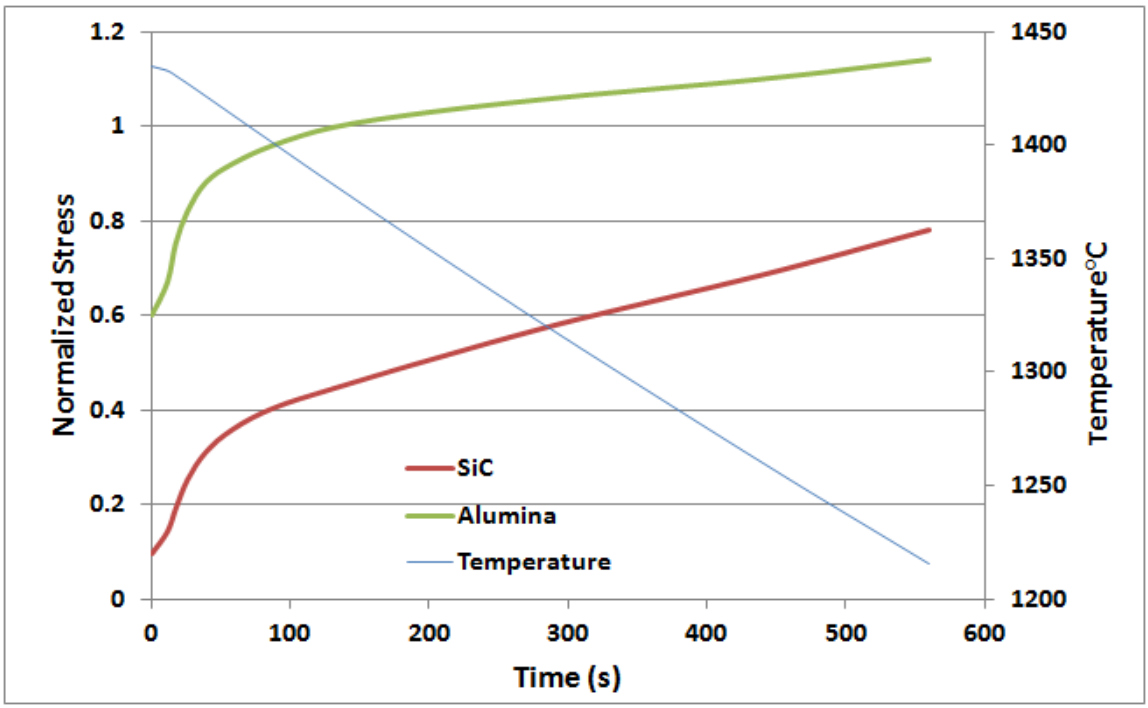

Figure 3-13. Comparison of stress developed for 50.8mm tubes –Cooling Phase

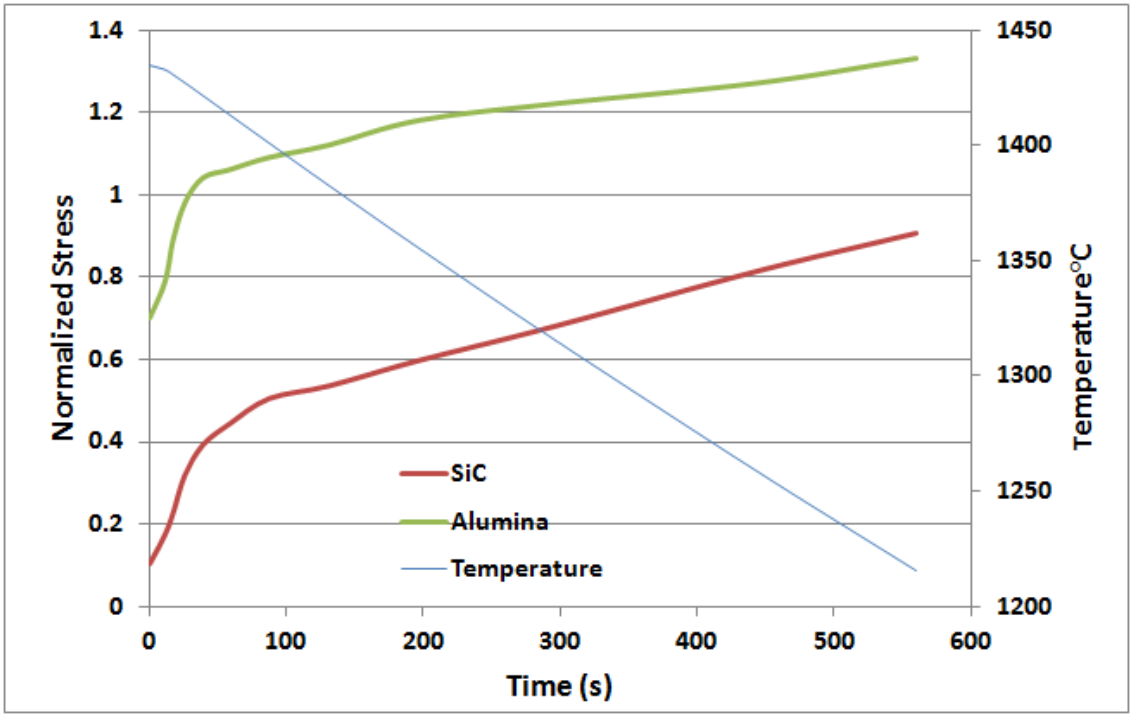

Figure 3-14. Comparison of stress developed for 76.2mm tubes –Cooling Phase

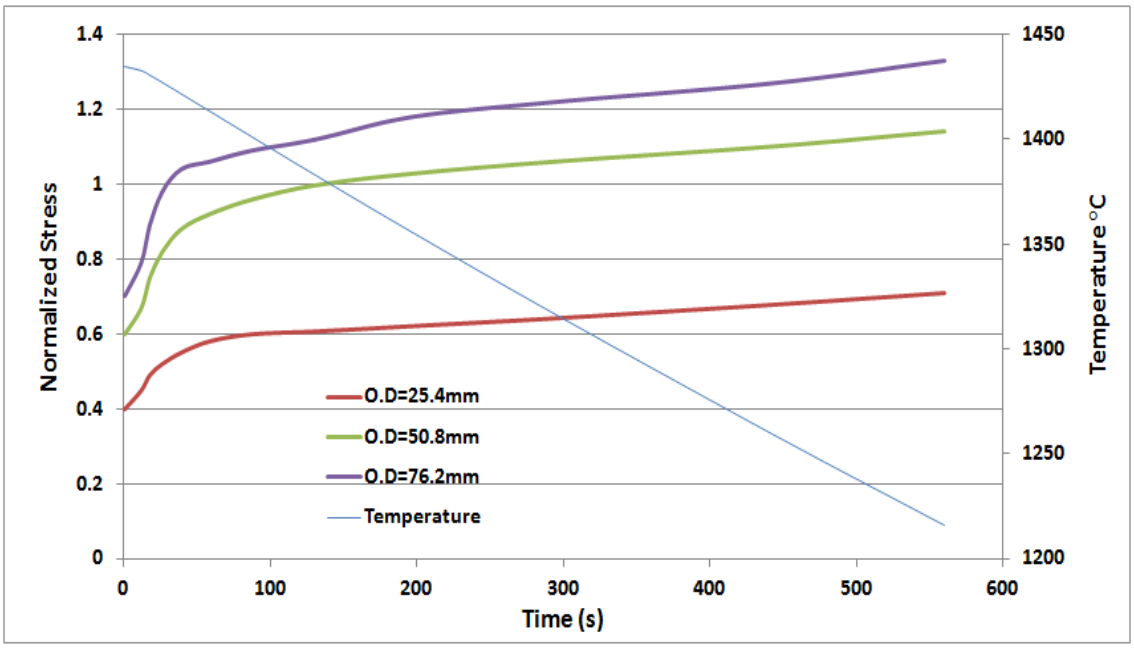

Figure 3-15. Comparison of stress developed for 3 different sizes of alumina tubes – Cooling Phase

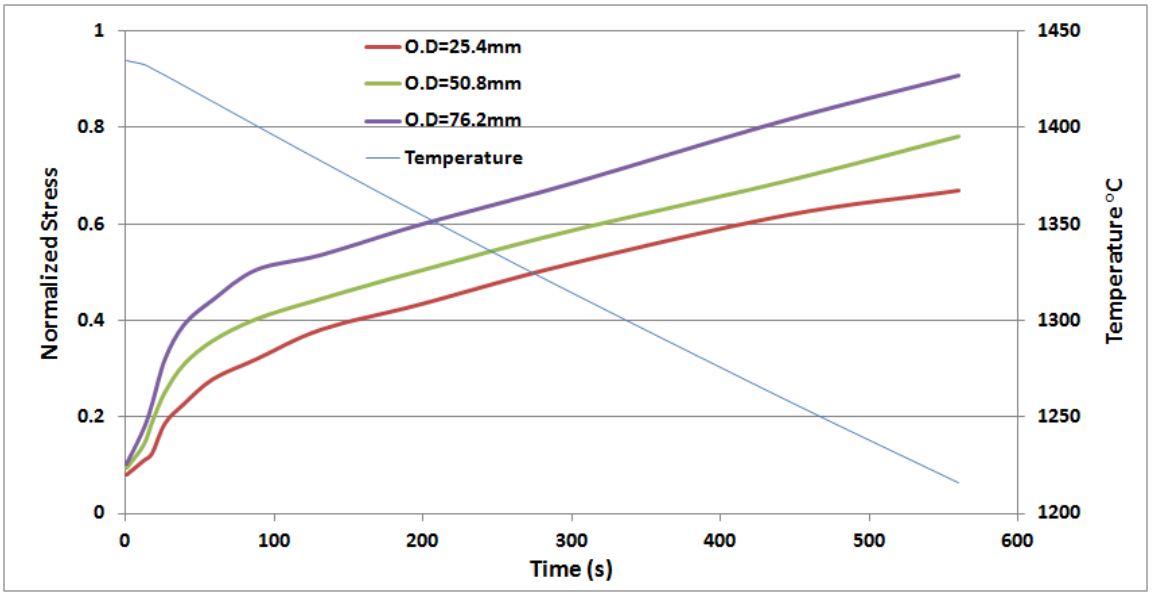

Figure 3-16. Comparison of stress developed for 3 different sizes of SiC tubes –Cooling Phase

The plots below show the stresses in heating phase of the cycle. Since the stress free temperatures are assumed to 1700°C and 2000°C, it is expected that the stresses will fall down during the heating phase.

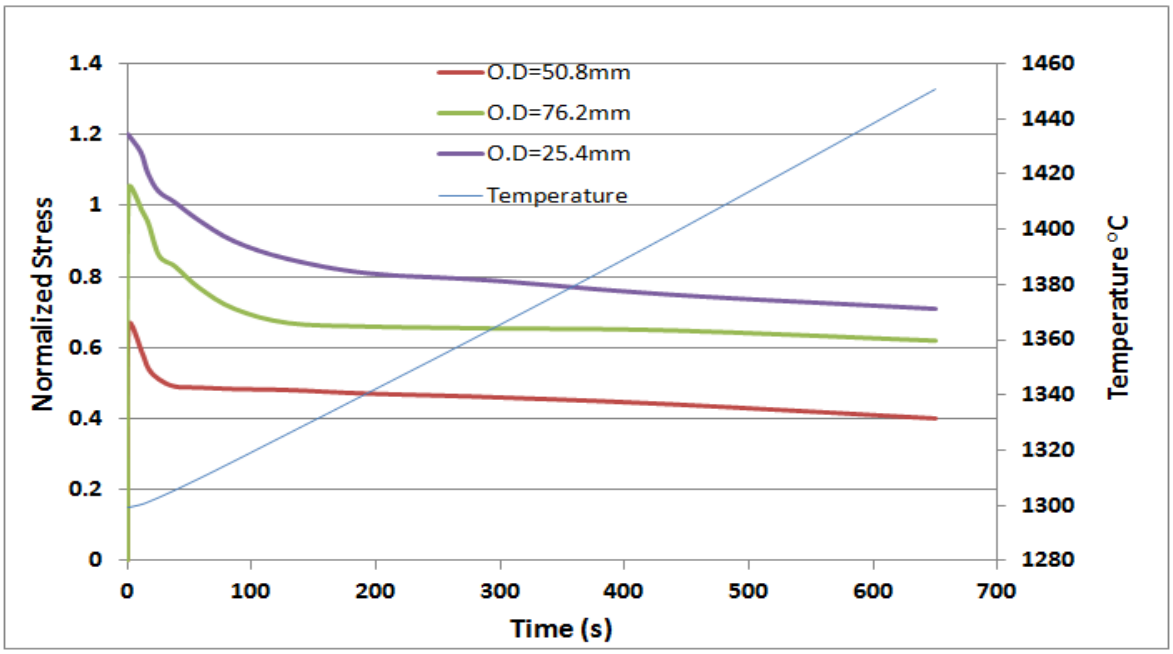

Figure 3-17. Comparison of stress developed for 3 different sizes of alumina tubes – Heating Phase

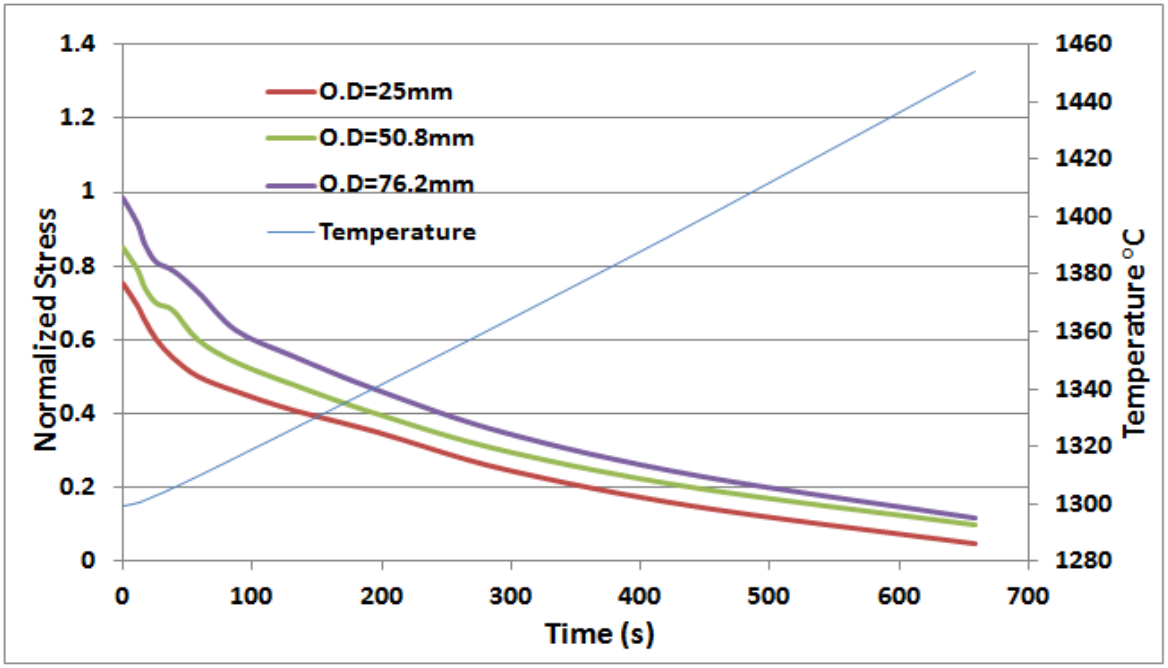

Figure 3-18. Comparison of stress developed for 3 different sizes of SiC tubes – Heating Phase

TSA on Other Components of the Reactor

Other component analyzed for thermal stress is the back plate of the reactor. Since the geometry of the back and front plate of the reactor is dependent on the tube size it is interesting to note how the stresses vary in the plates for different tube sizes. A TSA procedure similar to the tube was carried out for different back plate geometry. The idea is to check that for a given outer diameter of a back plate what will be the stresses in the geometry considering we fit the maximum number (as possible geometrically and ease of manufacturing)of tubes in the plate.

Assumptions for TSA in Back Plates

- Since the back plate always will receive direct radiation a constant flux of 7kW is assumed to hit a circular area with diameter of 5cm for the entire heating operation.
- It is assumed that the remaining area receives 1.5kW of uniform constant flux on account of diffuse radiation from other components within the cavity.
- During the heating phase the heat fluxes on the two different areas of the back plate are responsible for the temperature rise. During the cooling phase no heat flux acts on the back plate and it cools down primarily because of re-radiation to other cavity parts.
- The tube holes in the plate are assumed to be insulated.
- The tube holes are also assumed to be constrained for translational and rotational degree of freedom.

Following contour plots show the temperature profile in an Al_2O_3 back plate at the end of heating and cooling operations.

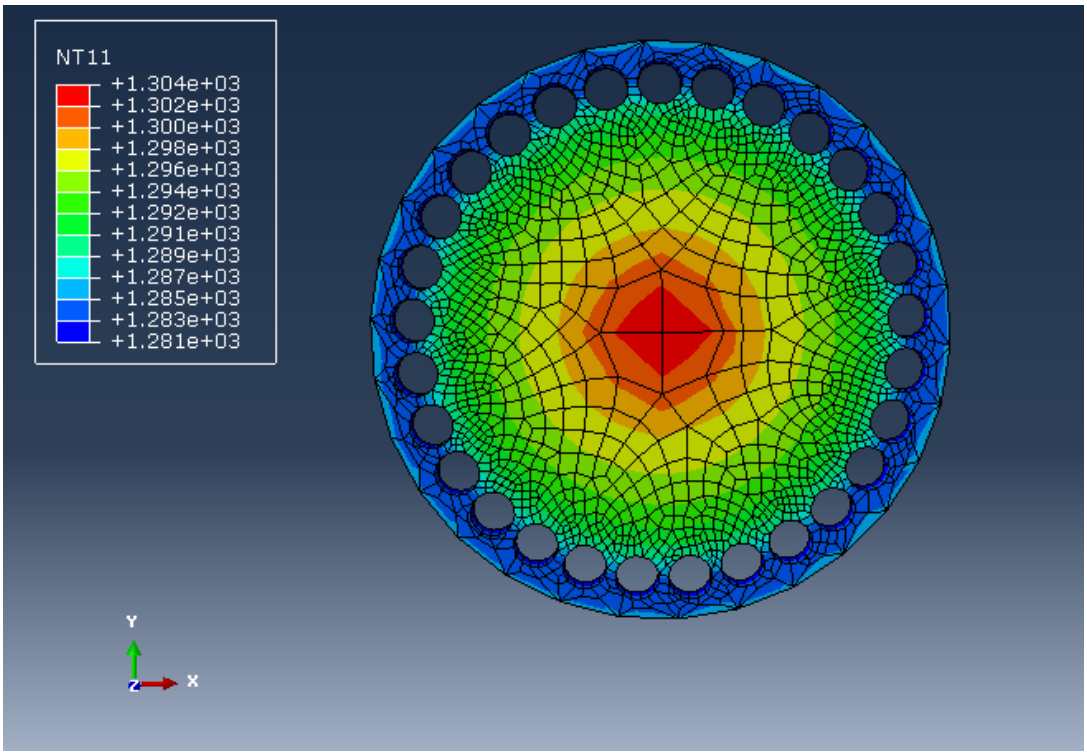

Figure 3-19. Temperature distribution on back plate made of fully dense alumina-Heating Phase

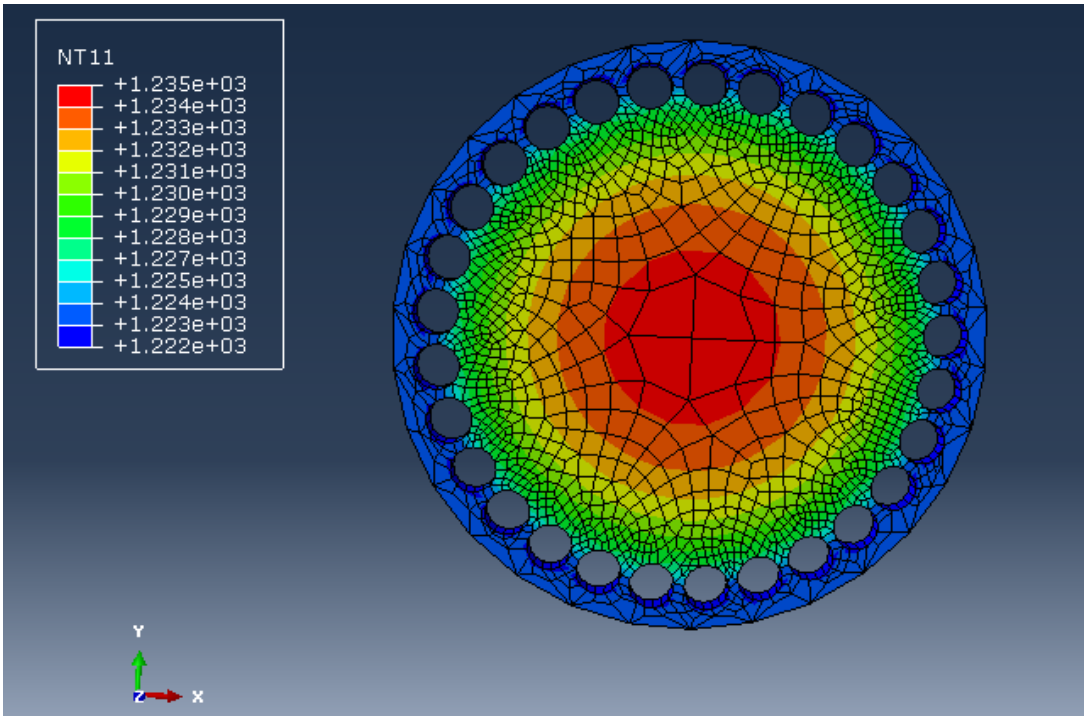

Figure 3-20. Temperature distribution on back plate made of fully dense alumina-Cooling Phase.

Corresponding to the above temperature profile the stresses in the back plate are shown in the following contour plots.

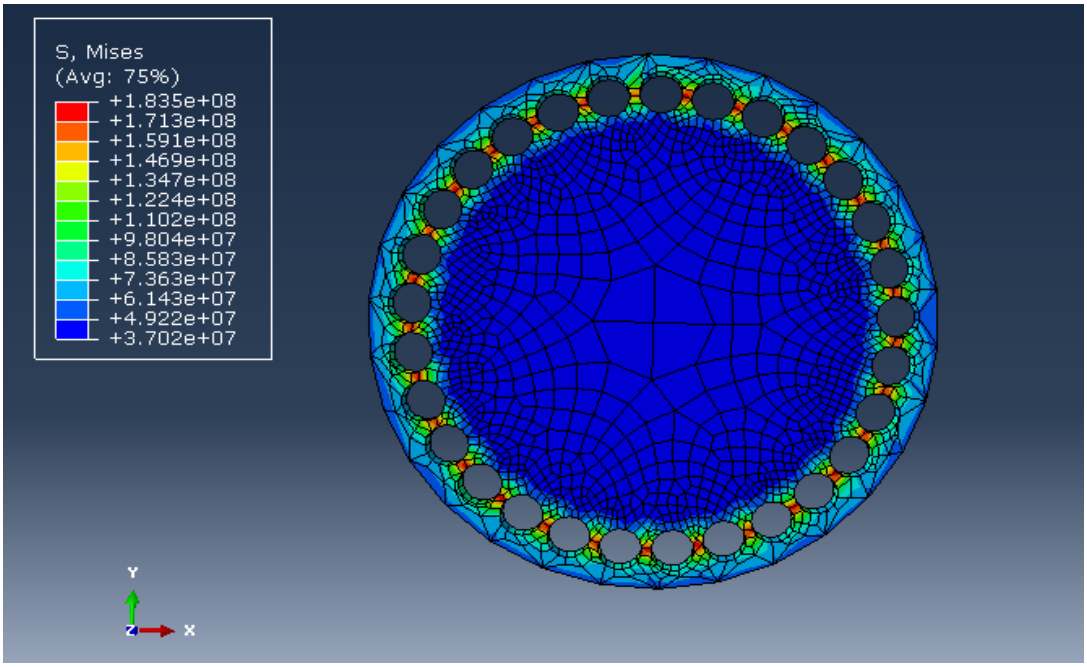

Figure 3-21. Stress distribution on back plate made of fully dense alumina-Heating Phase

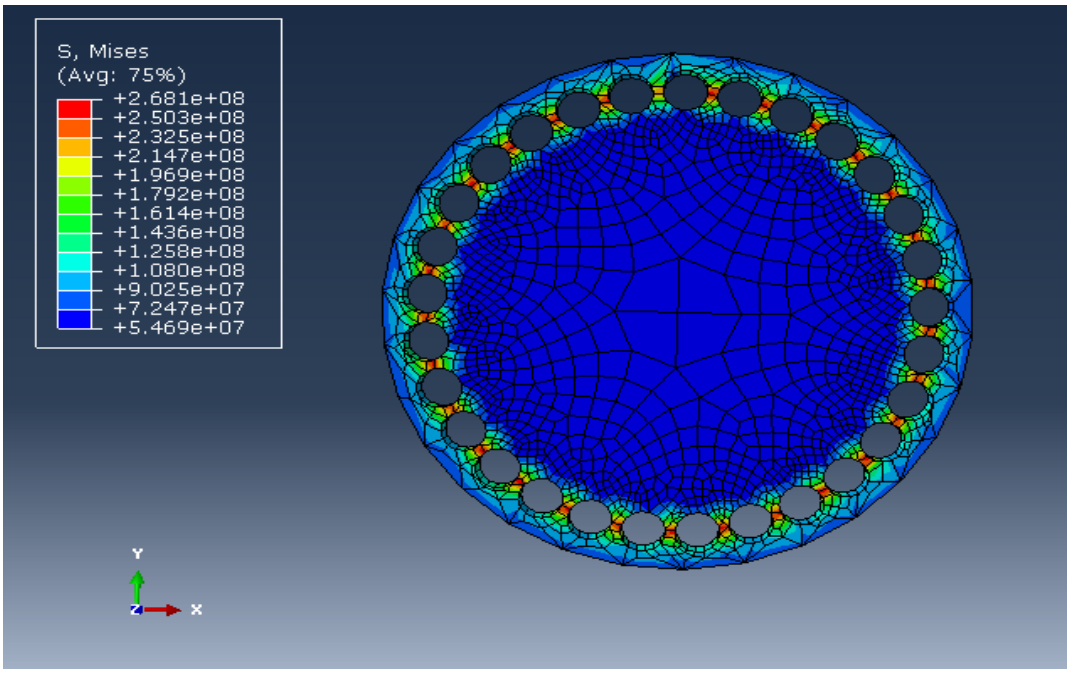

Figure 3-22. Stress distribution on back plate made of fully dense alumina-Cooling Phase

As seen from the above contour plots the critical stress limit of 130 MPA is exceeded during the heating phase itself indicating that the material could fail during heating. As expected the stresses are greater during the cooling phase. Experiments with similar geometry of alumina plates have shown that the cracks do occur at the places marked with highest stresses in the contour plots. This will be discussed in a later chapter again. Now, if we consider a similar plate which will house 76.2mm tubes following are the results that we get for Al_2O_3 plates.

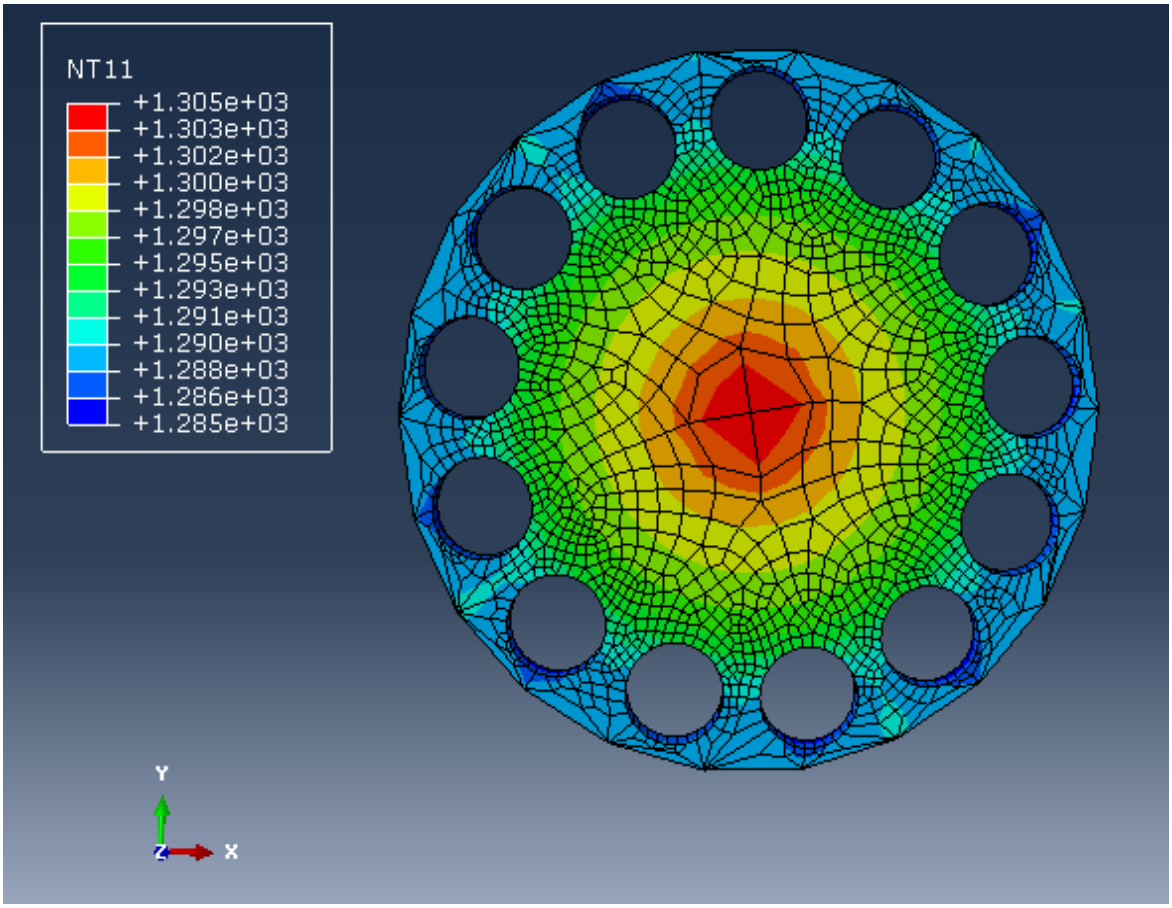

Figure 3-23. Temperature distribution on back plate with 76.2 mm diameter tube holes made of fully dense alumina-Heating Phase

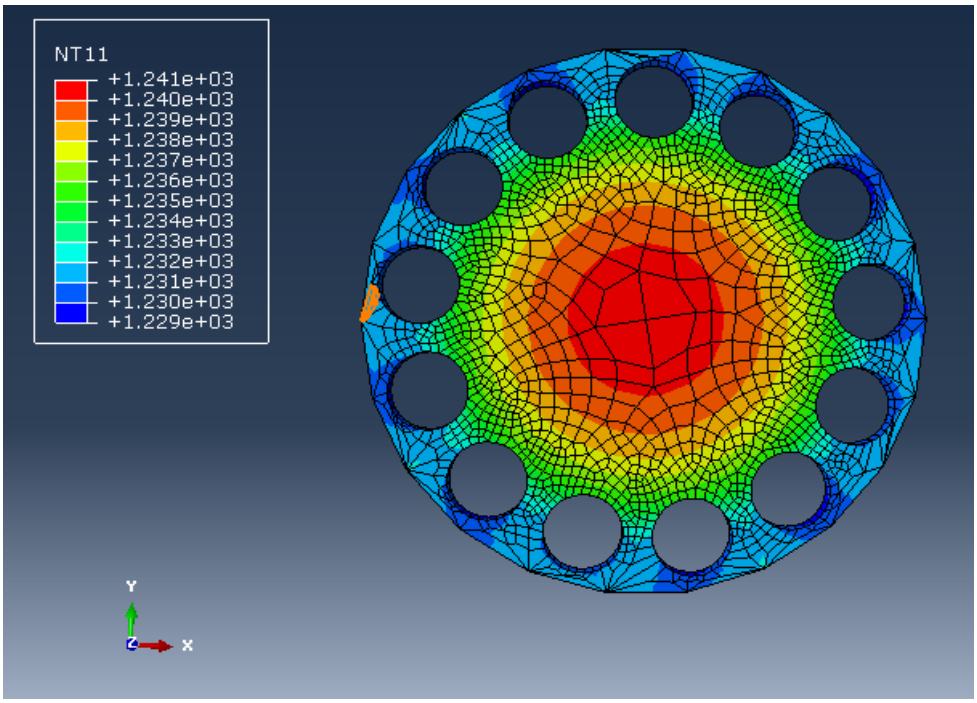

Figure 3-24. Temperature distribution on back plate with 76.2 mm diameter tube holes made of fully dense alumina-Cooling Phase

The related stresses developed in an Al_2O_3 plate are:

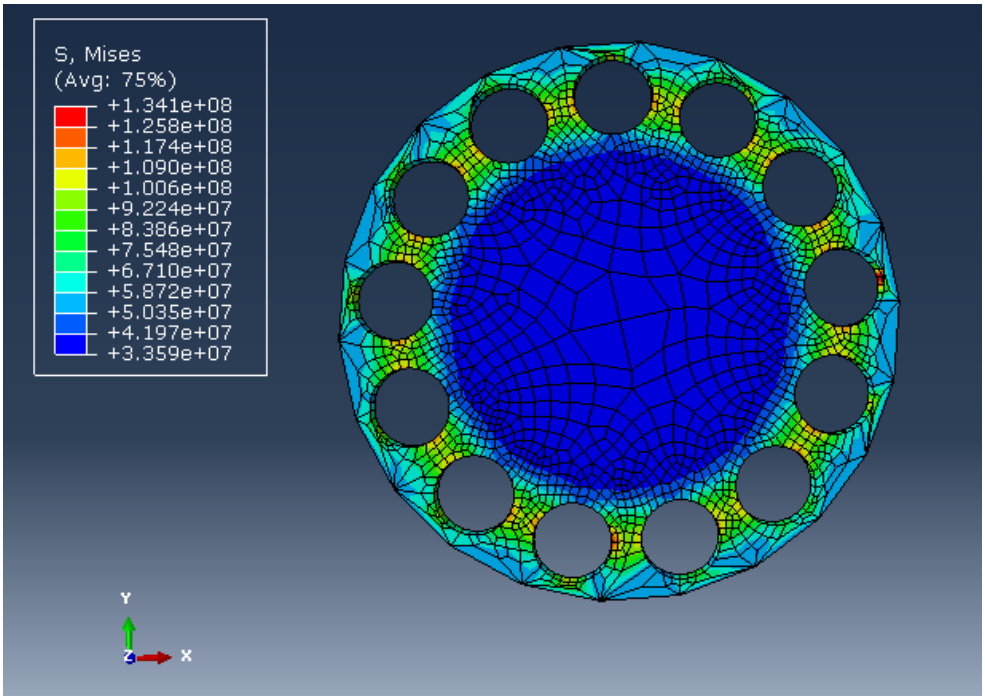

Figure 3-25. Stress distribution on back plate with 76.2 mm diameter tube holes made of fully dense alumina-Heating Phase

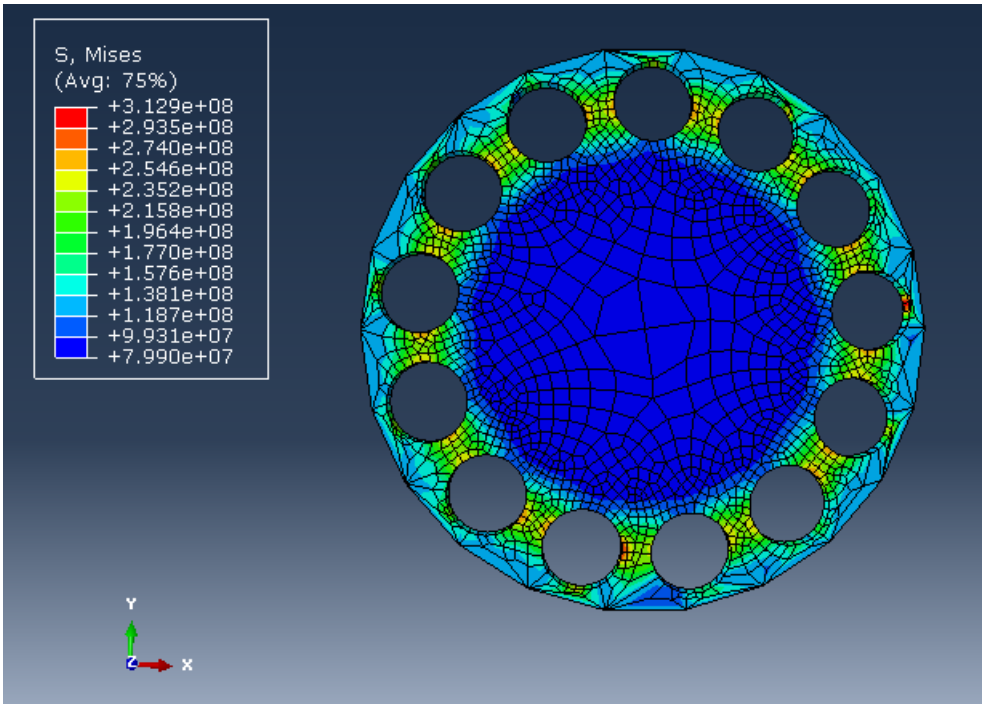

Figure 3-26. Stress distribution on back plate with 76.2 mm diameter tube holes made of fully dense alumina-Cooling Phase

In the above contours one can see that the critical stress for alumina is still well exceeded during the cooling stage and is almost equal to the failure value at 1500°C. Thus, as the tube size increases the stresses in the back plate will decrease.

CHAPTER 4
THERMAL TESTS WITH SOLAR SIMULATOR

Experimental Setup

The solar simulator at University of Florida consists of seven identical 3D ellipsoidal lamps that are aligned to have a common focal point. Each lamp has the ability to focus 7kW of thermal energy at a predetermined focal plane. The focal point lies in the Z plane of an XY table. The reactor or a flux target can be mounted on this table and the table can be controlled externally through a Labview program. On the XY table a flux target is mounted which can be used to create flux maps before or after the experiments. To capture the flux incident on the flux target there is an industrial grade CCD camera. The output of the camera, with post processing, can be viewed with the help of a MATLAB program.

(A) (B)

Figure 4-1. Ellipsoidal lamps at the solar simulator facility at UF. A) Front view B) Back view.

Figure 4-2. CCD camera at the solar simulator facility at UF

Solar Thermochemical Reactor

Construction

The reactor is constructed in 4 different parts: the front plate, back plate and two halves of a cylindrical body. As seen from Figure 4-4 below the two end plates have 29 tube holes for the tubes. Currently STCR is built for 29 25.4mm O.D tubes. The material for the STCR is Buster M-35 from Zircar Zirconia composed of 80% alumina and 20% silicates. The front plate has a 5 cm aperture which is aligned with the focal plane.

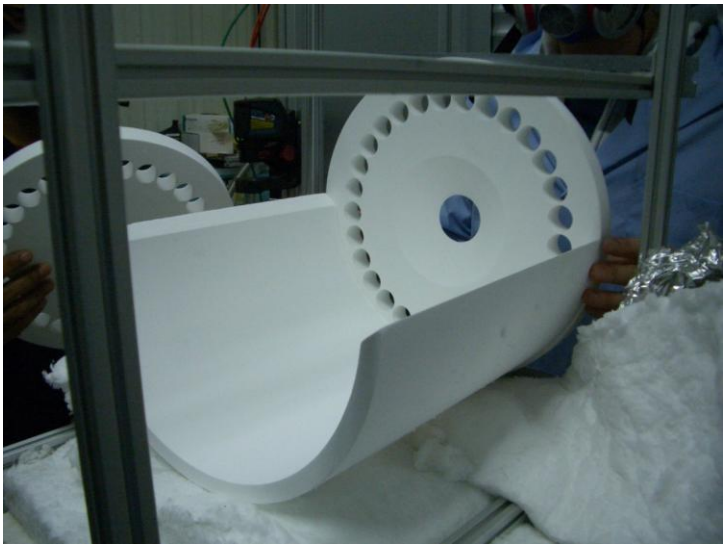

Figure 4-3. Different components of a STCR

STCR on the XY Table

To mount STCR on the XY table a separate frame was built off the XY table. This allowed the flexibility to move the focal plane of the reactor with the XY table. Whole of STCR was wrapped in 3 layers of 3cm thick glass wool insulation. The aperture of STCR was held fixed in the focal plane of the mirrors. This was done by gently pressing the STCR together with the help of metal strips pressed against the insulation cover. The STCR was mounted next to the flux target in such a way that during flux mapping operation STCR can be completely removed from the path of the light coming from the mirrors. A base of fire bricks was mounted on the metal base of the frame to prevent any damage to the frame due to excessive heat transfer.

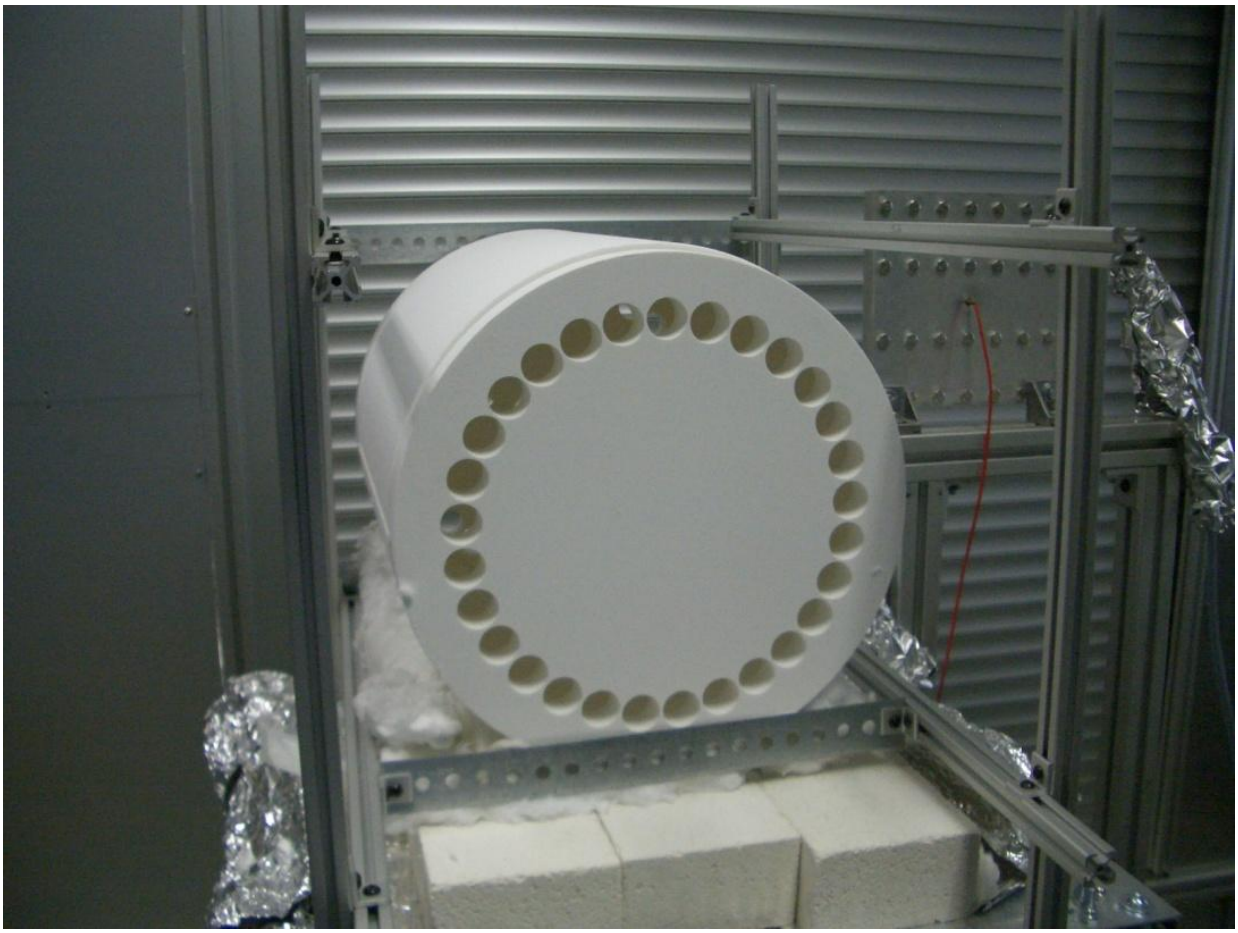

Figure 4-4. STCR kept on fire bricks

Figure 4-5. Assembly of STCR insulated with glass wool

Figure 4-6. Complete assembly of the STCR framework mounted on XY table

Finally, a shutter mechanism was created to prevent rapid cooling of the reactor during the shutdown stage. The shutter mechanism consists of a moving cam base (mounted on the reactor frame), a vertical structure and a fire brick covered with insulation (Figure 4-7). The idea behind the shutter is to cover the aperture of the reactor during the shutdown stage. Since, the reactor loses heat primarily by reradiating a shutter at the cavity can arrest the drastic drop of temperature within the cavity.

Experiments

Experiment 1

The first experiment was carried out without any tubes. In this experiment all the tube holes were closed with ceramic plugs (Figure 4-8). The basic idea behind this test was to test the ability of the structure to withstand thermal shock. It was pre-decided that the rate of change of temperature will be controlled to 10°C/min as closely as possible at least until working temperatures of 800°C were attained. Thermocouples were placed at different locations to log the temperature change. Of particular importance is the temperature history of the thermocouple which was placed at the center of the back plate. Since, TSA showed that the back plate will crack at the wedges between the holes, data from this particular thermocouple can be used to recalibrate the simulation model.

Results

After the test when the reactor was dissembled the back plate was found to have cracked on every wedge between any two tube holes. Also there was a major crack on the top of the back plate (Figure 4-9). The result of TSA also predicted stresses greater than the critical stresses at these on the wedges. However, it did not predict a major crack on the periphery of the back plate. Also, as stated before in Chapter 4 the stress

values predicted by TSA are probably over predicted. Hence, although TSA predicts a fracture of tubes at these locations in the actual experiments one can only observe cracks at the surface of the back plate and not a complete fracture of the component.

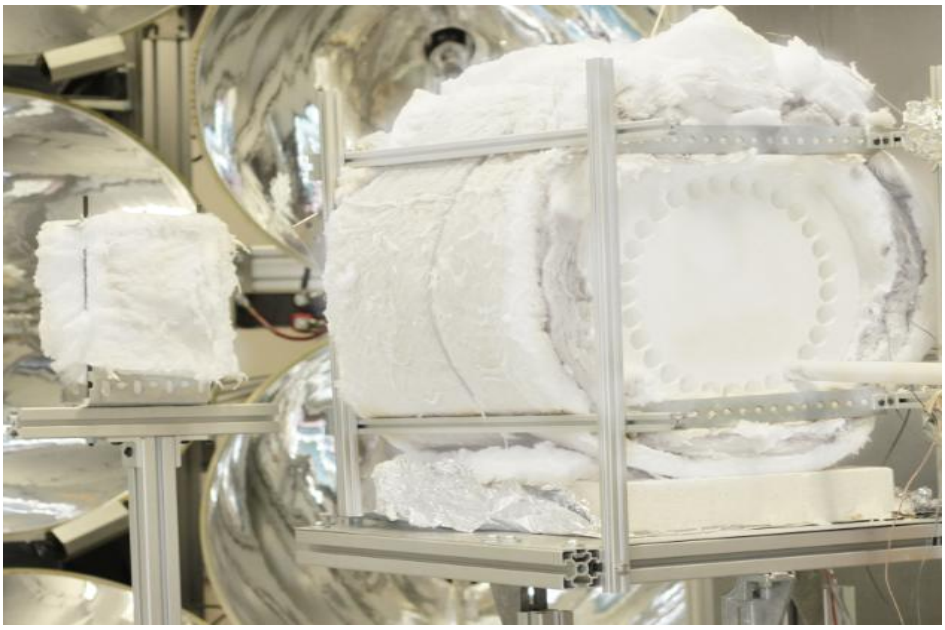

Figure 4-7. STCR with the shutter on the left

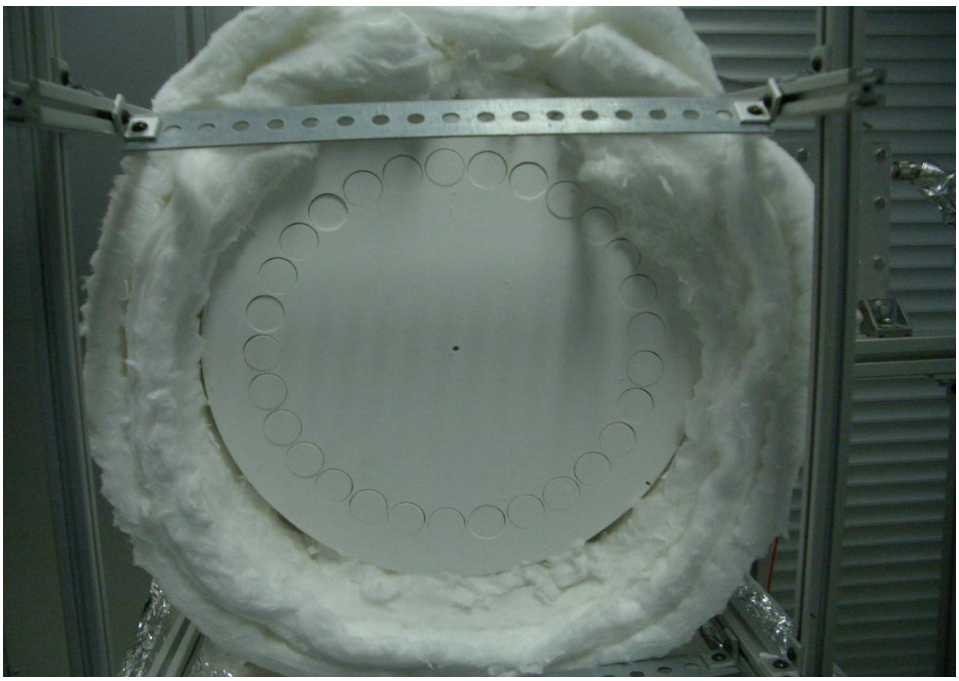

Figure 4-8. STCR with ceramic plugs on the back plate

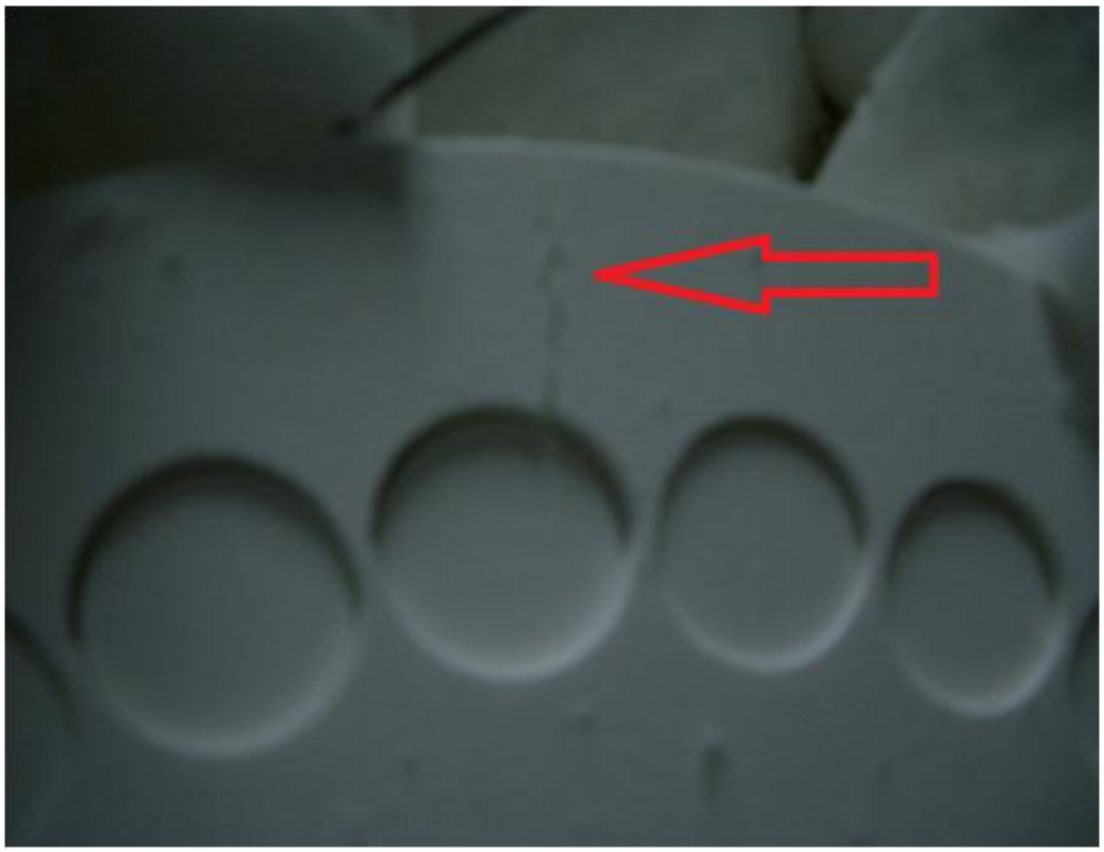

Figure 4-9. Crack at the periphery of the back plate of STCR

Experiment 2

The second experiment was carried out with one tube in the reactor. The basic idea behind this test was to determine the thermal robustness of the tube during a complete cycle of temperature. The tube is made of fully-dense alumina. It was placed in one of the bottom holes of the reactor. The average rate of heating and cooling was maintained at 10°C/ min at least till cycling temperature was attained. It is to be noted that much higher cycling temperatures (30°C-40°C / min) are desired in future. Since this was the first experiment with a tube in cavity a rate of 10°C/ min was chosen because it has been observed in other experiments(not related to solar simulator) that the alumina tubes, with similar properties, do not crack at this cycling rate.

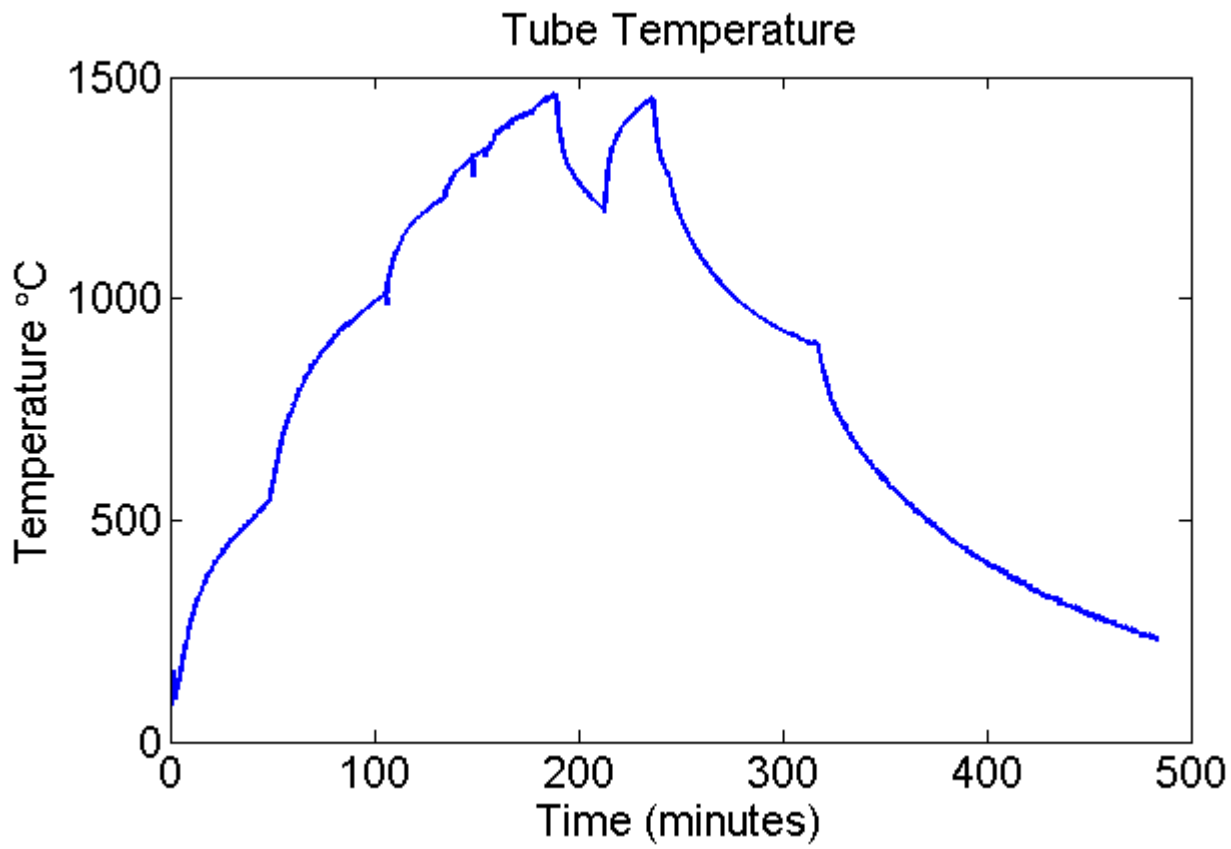

Figure 4-10. Time history of absorber tube's inside surface temperature

Results

During the experiment an average temperature change of 8.5°C/min was achieved in the heating phase. The graph (Figure 4-10) above shows the reading of the thermocouple which was placed inside the tube. As can be seen the temperatures do not increase linearly. This has to be taken into account in TSA simulations. At the end of the experiment there appeared be no visible cracks on the surface of the tubes although a much detailed inspection of the tube surface is pending. The TSA also predicted stress values lower than the critical values for 25.4mm alumina tubes. Therefore, faster temperature gradients can be tried during the cycling period while running the experiments. Similarly, appropriate changes can be made in the TSA to recalculate the stresses in the simulations.

Effectiveness of the Shutter to Prevent TS

While running the experiments in a solar simulator relatively good control was achieved over the temperature change during the heating phase by adjusting the lamps current and selecting the time when different lamps would turn on. As mentioned above, during the shutdown phase the shutter covers the aperture of the cavity and prevents drastic fall in temperature. The shutter was deployed after the last lamp was switched off. At this point the temperature of the tube was 720°C and the experiment had been running for approximately 320 minutes. What was observed was that the average temperature drop rate, after the deployment of shutter, was as low as of 5°C/min as compared to an average rate of 11°C/min before the shutter was deployed. . As was seen in TSA for 25mm O.D diameter alumina tubes a cooling rate of 20°C/min was acceptable because it did not cause critical stress values in the tube. The critical rate of cooling can hence be assumed to be at least greater than 20°C/min. Therefore, by using a shutter the temperature drop was kept well below the critical rate for cooling.

CHAPTER 5
CONCLUSIONS

Summary

An analysis to predict thermal stresses on two components of a STCR assembly has been presented. The analysis starts with preliminary investigation of flux mapping on different STCR designs using the Vegas Code. For the solar simulator facility available at UF the flux mapping results indicate the occurrence of hot spots for all designs and a heat loss through the cavity body. As a result, a design which consists of horizontal tubes arranged circumferentially on the inside surface of cavity body is chosen. By the results of an in-house code the temperature distribution on an absorber tube for this particular design is obtained. Using this data a TSA is carried out, for the cycling period of a STCR, based on some crucial assumptions. The most important of these are

The spatial distribution of temperatures is assumed to be fixed and only the amplitude of the temperatures changes. The material properties considered are those provided in published results of standard test specimen.

The current simulations are run for three different tube sizes for O.D. For each size two material of construction are considered: alumina and SiC. It is seen that alumina tubes of sizes 50.8mm and 76.2mm O.D the stresses developed are greater than the critical stresses at that temperature. For SiC stresses developed for 76.2 mm O.D exceed the critical stress values. It is also seen that SiC has the property of increasing flexural strength with increase in temperature which makes it an excellent candidate for high temperature application. Similar simulations were run for the back plate of the STCR. Simulations predicted the stress levels in the back plate to be higher

than the critical stress level. However, the material property used in simulation was for a dense alumina while in real experiments a fully dense alumina was not used.

Thermal tests were also carried out at the solar simulator at UF. During one of the tests it was observed that the back plate cracked at the place where simulations predicted thermal stress higher than the critical stresses. There was also a major crack on the periphery of the back plate which the simulations did not predict. In another test temperature profile on the inside surface of the tube was recorded. It was seen that the temperature does not vary linearly as was assumed in the simulation.

Current simulations results and experiments seem to suggest that SiC should be the preferred choice of tube materials because of increasing flexural strength. However, it remains to be seen how the simulations results will change when effects of creep, viscoelasticity and pre-existing flaws are taken under consideration.

Future Work

Looking forward, maximum cooling and heating rates of cavity and absorber tubes will be predicted considering the same assumptions that have been made in this analysis. These results can then be validated by experimentation in the solar simulator. Also, the present analysis covers only the stresses developed during the cycling phase of reactor operation. Similar analysis can be done for the startup heating phase and the shut down cooling phase, as and when temperature distribution profile (for absorber tubes)during these phase are available from the in-house code.

Most of the literature available on the TSA of ceramics suggests that standard material properties of ceramics, like those used in handbooks, should be avoided while predicting thermal stresses in a specimen of different geometric shape. This is so because specimens differ in their response to thermal stresses based on differences in

their microstructure, impurities and pre-existing flaws. Thus to get more accurate results, flexural strength tests must be carried out to achieve precise strength. Lastly, the effect of creep on stress relaxation and pre-existing flaws on stress concentration has to be considered to achieve simulation results which are close to real life scenario.

LIST OF REFERENCES

[1] 2009; The other kind of solar power, from http://www.economist.com/node/13725855

[2] Rodriguez L, Ana I, Marrero P, Gomez C. Comparison of solar thermal technologies for applications in seawater desalination. Desalination 2002; 142:135-142.

[3] Laing D, Steinmann WD, Viebahn P, Grater F, Bahl C. Economic analysis and life cycle assessment of concrete thermal energy storage for parabolic trough power plants. Journal of Solar Energy Engineering 2010; 132:10131-10136

[4] Meier A, Steinfeld A. Solar Thermochemical Production of Fuels. Advances in Science and Technology 2010; 74:303-312

[5] 2008, Industry Report, from www.solar-thermal.com

[6] Kutscher C, Mehos M, Turchi C, Glatzmaier G. Line-Focus Solar Power Plant Cost Reduction Plan. Milestone Report, Colorado National Renewable Energy Laboratory 2010

[7] Steinfeld A, Palumbo R. Solar Thermochemical Process Technology. Encyclopedia of Physical Science & Technology, R. A. Meyers Ed., Academic Press 2001;15: 237-256

[8] Noring J, Fletcher EA. High Temperature Solar Thermochemical Processing — Hydrogen and Sulfur from Hydrogen Sulfide Energy 1982; 7: 651-666.

[9] JANAF Thermochemical Tables National Bureau of Standards, 3rd ed., Washington D.C. 1985

[10] Charvin P, Abanades S, Beche E. Hydrogen production from mixed cerium oxides via three-step water splitting cycles. Solid State Ionics 2009; 180: 1003-1010

[11] Chueh W, Haile SM. Ceria as a thermochemical reaction medium for selectively generating syngas or methane from H_2O and CO_2. ChemSusChem 2009; 2: 735-741.

[12] Mehdizade M, Klausner JF, Barde A, Nima R, Mei R. Investigation of hydrogen production reaction kinetics for an iron-silica magnetically stabilized porous structure. Journal of Hydrogen Energy 2012; 37: 13263-13271

[13] Serpone N, Lawless D, Terzian R. Solar Fuels:Status and Perspectives. Solar Energy 1992;49:221-234.

[14] Lédé J. Solar thermochemical conversion of biomass, Solar Energy 1999; 65: 3-13.

[15] Perkins ,CM Synthesis gas production by rapid solar thermal gasification of corn stover , SPCE 2008; from NREL CD 550-42709

[16] Melchior T, Perkins C, Lichty P, Weimer AW, Steinfeld A. Solar –driven biochar gasification in a particle flow reactor. Chemical Engineering and Processing 2009 48, 1279-1287.

[17] Stamatiou A, Loutzenhiser PG, Steinfeld A.Solar Syngas Production viaH_2O/CO_2-Splitting Thermochemical Cycles with Zn/ZnO and FeO/Fe3O4 Redox Reactions. Chem. Mater. 2010; 22: 851–859

[18] Steinberg M. Fossil fuel decarbonization technology for mitigating global warming, International Journal of Hydrogen Energy 1999; 24: 771-777.

[19] Maag G, Zanganeh G, Steinfeld A. Solar thermal cracking of methane in a particle-flow reactor for the co-production of hydrogen and carbon, International Journal of Hydrogen Energy 2009; 34:7676 – 7685

[20] Meier A, Kirillov VA., Yu I, Reller A, Steinfeld A. Solar Thermal Decomposition of Hydrocarbons and Carbon Monoxide for the Production of Catalytic Filamentous Carbon, Chemical Engineering Science 1999; 54: 3341-3348.

[21] Palumbo R, Keunecke M, Steinfeld A. Reflections on the design of solar thermochemcial reactors: thoughts in transformation. Energy 2004; 29:727-744

[22] Hirsch D, Steinfeld A. Solar hydrogen production by thermal decomposition of natural gas using a vortex-flow reactor. International Journal of Hydrogen Energy 2004; 29: 47 – 55

[23] Ermanoski I, McDaniel A. 2012. Solar Hydrogen Production with a Metal Oxide Based Thermochemical Cycle, DOE Annual Merit Review, Project ID PD081

[24] Rodat S, Abanades S, Flamant G. Experimental Evaluation of Indirect Heating Tubular Reactors for Solar Methane Pyrolysis. International Journal of Chemical reactor Engineering 2010; 8: A25.

[25] Piatkowski N, Steinfeld A. Solar Gasification of Carbonaceous Waste Feedstocks in a Packed-Bed Reactor—Dynamic Modeling and Experimental Validation. AIChE 2011; 57: 3522-3533.

[26] Melchior T, Perkins C, Weimer A.W, Steinfeld A. A cavity receiver containing absorber for high temperature thermochemical processing using concentrated solar energy. International Journal of Thermal Science 2007; 47:1496-1503

[27] Melchior T, Steinfeld A. Radiative Transfer within a Cylindrical Cavity with Diffusely/Specularly Reflecting Inner Walls Containing an Array of Tubular Absorbers. International Journal of Solar Energy 2008; 130:021013-1-021013-8

[28] Modest, 2005, Thermal Radiation Heat Transfer, 3rd Ed., CRC press.

[29] Petrach, 2011, The Vegas Manual

[30] Richard K. Thermal Stresses-Advanced Theory and Applications, 1st Ed, Springer press 2008

[31] Carter J, Booker JR. Finite Element Analysis of Fully Coupled Thermoelasticity, Computer Structures 1989; 31: 73-80

[32] Kandil A, Kady A. Transient Thermal Stress Analysis of Thick Walled Cylinder, International Journal of Material Science 1995; 37: 721-732

[33] Akiyami S, Amada S. Estimation of Fracture Conditions of Ceramics by Thermal Shock with Laser Beams based on the Maximum Compressive Stress Criterion, International Journal of JSME 1992; 34: 91-94

[34] Lichty P, Steinfeld A. Solar Thermal Reactor Material Characterization, Solar Power and Chemical Energy Systems Symposium 1992; www.solarpaces.org.

[35] Hasselman L, Thermal Stress Resistance of Engineering Ceramics, Material Science and Engineering 1984; 71: 251-264

[36] Erikson B., Characterization of the University of Florida solar simulator and an inverse solution for identifying intensity distributions from multiple flux maps in concentrating solar applications, M.S Thesis, Department of Mechanical and Aerospace Engineering, University of Florida; 2012

BIOGRAPHICAL SKETCH

Nikhil Sehgal was born in New Delhi, India in 1986. He received his Bachelor of Science in mechanical engineering from University of Mumbai in 2009. He spent the next two years working as an engineer at Panasia Engineers Pvt. Ltd. and Sterling and Wilson Ltd respectively. During his time at Panasia Engineers Pvt. Ltd. he worked on design and development of novel refrigeration systems. He published an article in the ISHRAE Journal (Oct-2010) based on his work at Panasia Engineers Pvt. Ltd. Nikhil joined University of Florida in the fall of 2011. He started working on this project in January 2012. His present work involves testing the solar reactor at the solar simulator facility at UF. He received his MS from the University of Florida in the spring of 2013.